J. Fluid Mech. (2009), vol. 620, pp. 89–119. © 2009 Cambridge University Press
doi:10.1017/S0022112008004904 Printed in the United Kingdom

Steady separated flow past a circular cylinder at low Reynolds numbers

SUBHANKAR SEN[1], SANJAY MITTAL[2]† AND GAUTAM BISWAS[1]

[1]Department of Mechanical Engineering, Indian Institute of Technology Kanpur, Kanpur 208016, India
[2]Department of Aerospace Engineering, Indian Institute of Technology Kanpur, Kanpur 208016, India

(Received 26 March 2008 and in revised form 5 November 2008)

The steady two-dimensional laminar flow around a stationary circular cylinder has been investigated via a stabilized finite-element method. The Reynolds number Re is based on the cylinder diameter and free-stream speed. The results have been presented for $6 \leqslant Re \leqslant 40$ and the blockages between 0.000125 and 0.80. The blockage B is the ratio of the cylinder diameter to the domain width. There is large scatter in the value of Re_s, reported in the literature, marking the onset of the flow separation. From the present study the Re_s is found to be 6.29, approximately for $B = 0.005$. The effect of the blockage on the characteristic flow parameters is found to be insignificant for $B \leqslant 0.01$. The bubble length, separation angle and Re_s exhibit non-monotonic variation with the blockage. It is for the first time that such a behaviour for the separation angle and Re_s is being reported. Two types of boundary conditions at the lateral walls have been studied: the slip wall and towing tank. In general for high blockage, the results from the slip boundary condition are closer to the ones for the unbounded flow. In that sense, the use of the slip boundary condition as opposed to the towing tank boundary condition on the lateral walls is advocated. The bubble length, separation angle, base suction, total drag, pressure drag, viscous drag and maximum vorticity on the cylinder surface for the steady flow are found to vary as Re, $Re^{-0.5}$, Re^{-1}, $Re^{-0.5}$, $Re^{-0.64}$, $Re^{-0.60}$ and $Re^{0.5}$, respectively. The extrapolated results for the steady flow, for higher Re, are found to match quite well with the other results from the literature.

1. Introduction

The incompressible flow past a stationary cylinder is a classical bluff body problem in fluid mechanics. Its enriched physics and real-life applications have attracted the attention of the engineers and scientists for over a century, leading to many theoretical and experimental investigations. Despite its simple geometry, the flow past a circular cylinder is considered to be a baseline case of more complex flows (Zdravkovich 1997).

To this day, there is no agreement on the exact value of the laminar separation Reynolds number, Re_s, for the steady unbounded flow. The dependence of Re_s, for confined flow, on the boundary conditions and blockage has received little attention in the past. The blockage, B, due to the cylinder is defined as the ratio of the cylinder

† Email address for correspondence: smittal@iitk.ac.in

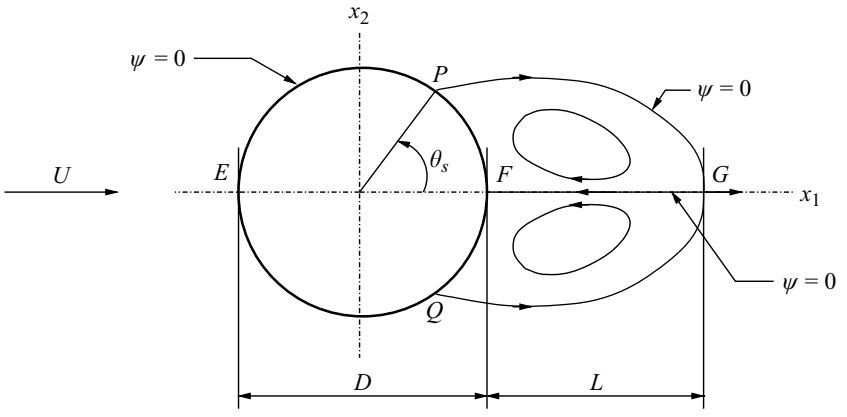

E = Forward stagnation point
F = Rear stagnation point or base point
G = Wake stagnation point
P, Q = Separation points

FIGURE 1. Schematic representation of the cylinder and separation bubble cross-section.

diameter D to the width H of the experimental apparatus or computational domain. In the present work we conduct a systematic numerical investigation to address the dependence of Re_s and numerical treatment of the boundary conditions on the lateral walls. Recent numerical investigations involving the blockage effect on the flow field of a circular cylinder at low Re include Kumar & Mittal (2006*a*,*b*) and Prasanth *et al.* (2006). Kumar & Mittal (2006*a*,*b*) investigated the effect of the blockage on the vortex shedding frequency and the critical Reynolds number Re_c leading to the vortex shedding. Prasanth *et al.* (2006) studied the blockage effect on the flow field of a freely vibrating cylinder at low Re.

Before proceeding to the current numerical work, we describe the structure of the separation bubble or standing vortex pair and present an outline of the previous experimental, numerical, analytical and semi-analytical investigations involving this flow by different researchers. A schematic of the steady separation bubble is shown in figure 1. The flow is from left to right. The key geometrical parameters of interest that characterize the separation bubble are the bubble length L and separation angle θ_s (expressed in degrees). The separation angle θ_s is measured in a counterclockwise direction from the rear stagnation point or base point F. The bubble length (also called eddy length) is defined as the distance measured along the wake centreline between the base point, F, and the wake stagnation point G. The two symmetric, counter-rotating recirculation zones remain stably attached to the cylinder till the initiation of the vortex shedding.

Nisi & Porter (1923) conducted a pioneering investigation to determine the separation Reynolds number and found $Re_s = 3.2$. Their experimental investigations were based on smoke visualization. Using oil as the working fluid, Homann (1936) studied the flow around the cylinders and provided flow visualization pictures between $Re = 1.95$ and $Re = 140.5$. He estimated $Re_s = 6$ for $B = 0.067$. Taneda (1956) conducted experiments in a towing tank. From the plot of the eddy length with Re, he determined $Re_s = 5$ by extrapolation. Grove *et al.* (1964) and Acrivos *et al.* (1965, 1968) conducted a series of oil tunnel experiments for the steady

separated flow. For the constant blockage, these experiments consistently showed linear variation of the bubble length with Re even in the presence of a splitter plate. A shorter bubble with the wall proximity was also noted. Nishioka & Sato (1974) conducted wind tunnel experiments and determined the detailed structure of the wake velocity distribution for Re in the range of 10–80. Coutanceau & Bouard (1977) employed flow visualization to explore the closed wake structure and its evolution with Re for $5 < Re < 40$ in the towing tank experiments. The Re_s estimated by Coutanceau & Bouard (1977) is 4.4 for the unbounded flow. In their experiments, λ was the ratio of the cylinder and tank diameters. The value of Re_s was found to increase while the eddy length and separation angle decrease with increasing λ.

The early numerical investigations mainly employed the streamfunction–vorticity (ψ–ω) formulation of the Navier–Stokes equations and the finite-difference discretization method. The numerical solutions obtained by integrating the steady-state equations include the works of Thom (1933) at $Re = 10$ and 20, Kawaguti (1953) at $Re = 40$ and Apelt (1961) at $Re = 40$ and 44. All these studies consistently indicated an approximate linear growth of the standing vortex pair with Re. The results produced by Allen & Southwell (1955) in the range of $Re = 0$–10^3 exhibit a tendency towards reduced bubble length for some Re between 10 and 100. The work of Hamielec & Raal (1969) also predicts an ultimate decrease of the bubble length beyond $Re = 50$. Takami & Keller (1969) solved the ψ–ω equations up to $Re = 60$ on a transformed grid by finite-difference-type discretization and estimated $Re_s < 7$. This work was an extension of the earlier investigation by Keller & Takami (1966) for the Reynolds number range of 2–15.

Following a finite-difference discretization of the time-dependent ψ–ω equations, Kawaguti & Jain (1966) explored the flow for $Re = 1$ to 100 and reported the steady-state solutions in the range of $Re = 10$–50. The length of the standing eddy at $Re = 50$ was overpredicted. Thoman & Szewczyk (1969) solved the time-dependent ψ–ω equations on a hybrid grid. Though they documented results for Re ranging from 1 to 3×10^5, owing to the inadequate domain size, the low Re solutions were influenced by the wall effects. Son & Hanratty (1969) provided finite-difference solutions based on the ψ–ω formulation for $Re = 40$, 200 and 500. Based on numerical investigations, Pruppacher, Clair & Hamielec (1970) concluded that the standing eddy begins to develop at $Re_s \approx 5$. Tuann & Olson (1978) performed one of the earliest finite-element simulations for the flow past a circular cylinder at low Re. The simulations were based on the ψ–ω formulation, and they also concluded that $Re_s \approx 5$. Fornberg (1980, 1985, 1991) conducted extensive numerical investigations for the steady flow past a circular cylinder up to $Re = 800$. An approximate linear growth of the eddy with the Reynolds number was observed. Following a penalty finite-element formulation, Chen (2000) determined Re_s at blockages 0.10 and much larger subject to different boundary conditions (see table 1). A monotonic increase of Re_s with the blockage was observed in each case. Wu *et al.* (2004) conducted towing tank experiments and spectral-element investigations for the Reynolds number range of 7–280. They predicted smaller θ_s with increasing blockage and also suggested that the laminar separation commences at $Re_s > 6$.

The initial theoretical studies to determine the separation Reynolds number were conducted by Tomotika & Aoi (1950) and Yamada (1954). Based on the asymptotic theory, Smith (1979) predicted the behaviour of various characteristic flow parameters for the steady laminar flow past a circular cylinder. The numerical solutions of Fornberg (1980) for Re up to 300 were compared with theory in a later paper by

Studies	Method[a]	B	Re_s
Nisi & Porter (1923)	Experiments (smoke visualization)		3.2
Homann (1936)	Experiments	0.067	6
Taneda (1956)	Experiments (in towing tank)	0.03	5
Takami & Keller (1969)	Numerical (FDM on $\psi-\omega$ equations)		< 7
Underwood (1969)	Semi-analytical		5.75
Dennis & Chang (1970)	Semi-analytical		6.2
Pruppacher *et al.* (1970)	Numerical		≈ 5
Nieuwstadt & Keller (1973)	Semi-analytical		≈ 7
Coutanceau & Bouard (1977)	Experiments (in towing tank)	0	4.4
		0.024	5.2
		0.07	7.2
		0.12	9.6
Tuann & Olson (1978)	Numerical (FEM on $\psi-\omega$ equations)		≈ 5
Chen (2000)	Numerical (penalty FEM)	0.1[b]	6.9
		0.1[c]	4.6
		0.1[d]	6.2
Wu *et al.* (2004)	Experiments (in towing tank) and numerical (SEM)		> 6

[a] FDM, finite-difference method; FEM, finite-element method; SEM, spectral-element method.
[b] Flow between two stationary infinite plates ($0.10 \leqslant B \leqslant 0.95$).
[c] Flow between two stationary semi-infinite plates ($0.10 \leqslant B \leqslant 0.95$).
[d] Towing tank boundary condition ($0.10 \leqslant B \leqslant 0.70$).

TABLE 1. Summary of the separation Re for the steady flow past a circular cylinder as proposed by different researchers.

Smith (1981). A satisfactory agreement for various flow parameters was found except for the bubble length.

Based on the semi-analytical approach, Dennis & Shimshoni (1965) provided results for $Re = 0.01$–10^6. Their results show an increase in L with Re for low Re. Beyond $Re \approx 30$, they reported a decrease in the bubble length. This observation is in stark contrast to the general agreement that L increases with increasing Re. Following a semi-analytical method of series truncation for the Navier–Stokes equations of motion, Underwood (1969) presented results for $Re = 0.4$–10 and found $Re_s = 5.75$. Following a ψ–ω formulation, Dennis & Chang (1970) predicted Re_s to exist between 5 and 7 and estimated its value as 6.2. By employing finite Fourier series approximations for ψ and ω, Nieuwstadt & Keller (1973) solved the steady ψ–ω equations and reported results for $Re = 1$–40. They concluded that $Re_s \approx 7$.

The separation Reynolds numbers reported by various studies in the past and relevant information are listed in table 1. Large scatter in the value of Re_s, which ranges from 3.2 to 7, is seen. To our knowledge, there is no systematic investigation of the evolution of Re_s with respect to the blockage except the experimental work of Coutanceau & Bouard (1977) and the recent numerical work of Chen (2000). However, the investigation of Chen (2000) does not include the $B < 0.10$ cases for the prediction of Re_s. One of the objectives of the present study is to determine the Re_s for the unbounded flow. We are also interested in investigating the dependence of Re_s on the blockage and boundary conditions for the confined flow.

A stabilized finite-element method with equal order bilinear interpolation for the velocity and pressure has been used. The computational domain has been discretized

using a block structured, non-uniform mesh. At high Re, in an advection-dominated flow, the Galerkin formulation of the flow equations leads to node-to-node oscillations in the velocity field. This numerical instability is overcome by adding the streamline-upwind/Petrov–Galerkin (SUPG) stabilization terms. The SUPG formulation for the convection-dominated flows was introduced by Hughes & Brooks (1979) and Brooks & Hughes (1982). The pressure-stabilizing/Petrov–Galerkin (PSPG) stabilization terms are added to the formulation to enable the use of equal-order interpolation for the velocity and pressure. Hughes, Franca & Balestra (1986) introduced the pressure stabilization methods in the context of Stokes flow, and Tezduyar *et al.* (1992) generalized the method to finite Reynolds number flows.

The outline of the rest of the paper is as follows: In § 2, the governing equations for an incompressible fluid flow are reviewed. The finite-element formulation involving the SUPG and PSPG stabilizations is presented in § 3. The definition of the problem and the finite-element mesh are described in §§ 4 and 5, respectively. The validation of the formulation and its implementation are discussed in § 6. The pressure distribution on the surface of the cylinder and the drag coefficient are compared with the earlier results, and excellent agreement is observed. The domain extent and mesh convergence studies are also presented in the same section. The main results are presented and discussed in § 7. The effect of the blockage, boundary conditions and Re on the characteristic flow quantities is studied. Also, the separation Reynolds number is determined for the unbounded and confined flow. Finally, empirical relations are proposed for various flow parameters and utilized to predict the flow characteristics at higher Re. In § 8, a few concluding remarks are made.

2. The governing equations

Let $\Omega \subset \mathbb{R}^{n_{sd}}$ be the spatial domain, where $n_{sd} = 2$ is the number of space dimensions. The boundary of Ω is denoted by Γ and is assumed to be piecewise smooth. The closure of the domain is denoted by $\overline{\Omega}$. The spatial coordinates are denoted by $\boldsymbol{x}$. The equations governing the steady flow of an incompressible fluid of density, ρ, are

$$\rho(\boldsymbol{u}\cdot\boldsymbol{\nabla}\boldsymbol{u} - \boldsymbol{f}) - \boldsymbol{\nabla}\cdot\boldsymbol{\sigma} = 0 \text{ on } \Omega, \tag{2.1}$$

$$\boldsymbol{\nabla}\cdot\boldsymbol{u} = 0 \text{ on } \Omega. \tag{2.2}$$

Here $\boldsymbol{u}$, $\boldsymbol{f}$ and $\boldsymbol{\sigma}$ denote the fluid velocity, body force per unit volume and the Cauchy stress tensor, respectively. The stress is the sum of its isotropic and deviatoric parts:

$$\boldsymbol{\sigma} = -p\boldsymbol{I} + \boldsymbol{T}, \quad \boldsymbol{T} = 2\mu\boldsymbol{\varepsilon}(\boldsymbol{u}), \quad \boldsymbol{\varepsilon}(\boldsymbol{u}) = \tfrac{1}{2}((\boldsymbol{\nabla}\boldsymbol{u}) + (\boldsymbol{\nabla}\boldsymbol{u})^T), \tag{2.3}$$

where p, $\boldsymbol{I}$, μ and $\boldsymbol{\varepsilon}$ are the pressure, identity tensor, dynamic viscosity of the fluid and strain rate tensor, respectively. Both, the Dirichlet- and Neumann-type boundary conditions are accounted for and are represented as

$$\boldsymbol{u} = \boldsymbol{g} \text{ on } \Gamma_g, \quad n\cdot\boldsymbol{\sigma} = \boldsymbol{h} \text{ on } \Gamma_h, \tag{2.4}$$

respectively, where Γ_g and Γ_h are the complementary subsets of the boundary Γ; n is its unit normal vector; and $\boldsymbol{h}$ is the surface traction vector. In the present simulations we have mainly employed two different kinds of boundary conditions on the lateral walls of the domain, namely the slip and towing tank boundary conditions (see figure 2). In the slip boundary condition, the component of the velocity normal to and the component of the surface traction vector along the upper and lower boundaries are prescribed a zero value. In contrast, the towing tank boundary condition involves

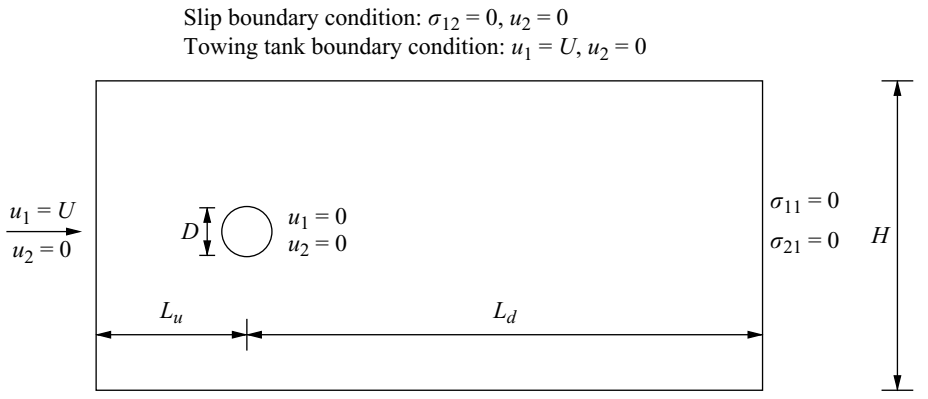

FIGURE 2. Problem definition for flow past a stationary circular cylinder.

the free-stream speed condition on the lateral boundaries. The no-slip boundary condition is applied on the surface of the cylinder. The free-stream condition on the velocity is prescribed on the upstream boundary. To enable comparison with the results of Sahin & Owens (2004) for the confined flow with high blockage (up to $B = 0.90$), a third type of boundary condition that involves the no-slip sidewalls and parabolic inlet is employed. For all the three types of boundary conditions, a Neumann condition for the velocity is specified at the downstream boundary that corresponds to the stress-free condition.

3. The finite-element formulation

The spatial domain Ω is discretized into the non-overlapping subdomains Ω^e, $e = 1, 2, \ldots, n_{el}$, where n_{el} is the number of elements. Let $\mathscr{S}_{\boldsymbol{u}}^h$ and $\mathscr{S}_p^h$ be the finite-dimensional trial function spaces for the velocity and pressure, respectively, and the corresponding weighting function spaces are denoted by $\mathscr{V}_{\boldsymbol{u}}^h$ and $\mathscr{V}_p^h$. These function spaces are defined as

$$\mathscr{S}_{\boldsymbol{u}}^h = \{\boldsymbol{u}^h | \boldsymbol{u}^h \in [H^{1h}(\Omega)]^2, \boldsymbol{u}^h \doteq \boldsymbol{g}^h \text{ on } \Gamma_g\}, \tag{3.1}$$

$$\mathscr{V}_{\boldsymbol{u}}^h = \{\boldsymbol{w}^h | \boldsymbol{w}^h \in [H^{1h}(\Omega)]^2, \boldsymbol{w}^h \doteq 0 \text{ on } \Gamma_g\}, \tag{3.2}$$

$$\mathscr{S}_p^h = \mathscr{V}_p^h = \{q^h | q^h \in H^{1h}(\Omega)\}, \tag{3.3}$$

$$\text{where } H^{1h} = \{\phi^h | \phi^h \in C^0(\overline{\Omega}), \phi^h \in P^1 \forall \Omega^e\}. \tag{3.4}$$

Here, P^1 represent the first-degree polynomials. The stabilized finite-element formulation of the conservation equations (2.1) and (2.2) is written as follows: find $\boldsymbol{u}^h \in \mathscr{S}_{\boldsymbol{u}}^h$ and $p^h \in \mathscr{S}_p^h$ such that $\forall \boldsymbol{w}^h \in \mathscr{V}_{\boldsymbol{u}}^h$, $q^h \in \mathscr{V}_p^h$,

$$\begin{aligned}
&\int_\Omega \boldsymbol{w}^h \cdot \rho(\boldsymbol{u}^h \cdot \boldsymbol{\nabla}\boldsymbol{u}^h - \boldsymbol{f})\,\mathrm{d}\Omega + \int_\Omega \boldsymbol{\varepsilon}(\boldsymbol{w}^h) : \boldsymbol{\sigma}(p^h, \boldsymbol{u}^h)\,\mathrm{d}\Omega + \int_\Omega q^h \boldsymbol{\nabla}\cdot\boldsymbol{u}^h\,\mathrm{d}\Omega \\
&\quad + \sum_{e=1}^{n_{el}} \int_{\Omega^e} \frac{1}{\rho}(\tau_{SUPG}\rho\boldsymbol{u}^h \cdot \boldsymbol{\nabla}\boldsymbol{w}^h + \tau_{PSPG}\boldsymbol{\nabla}q^h).[\rho(\boldsymbol{u}^h \cdot \boldsymbol{\nabla}\boldsymbol{u}^h - \boldsymbol{f}) - \boldsymbol{\nabla}\cdot\boldsymbol{\sigma}(p^h, \boldsymbol{u}^h)]\,\mathrm{d}\Omega^e \\
&\quad + \sum_{e=1}^{n_{el}} \int_{\Omega^e} \delta\boldsymbol{\nabla}\cdot\boldsymbol{w}^h \rho\boldsymbol{\nabla}\cdot\boldsymbol{u}^h\,\mathrm{d}\Omega^e = \int_{\Gamma_h} \boldsymbol{w}^h \cdot \boldsymbol{h}^h\,\mathrm{d}\Gamma.
\end{aligned} \tag{3.5}$$

In the variational formulation given by (3.5), the first three terms and the right-hand side constitute the Galerkin formulation of the problem. The first series of element level integrals are the SUPG and PSPG stabilization terms added to the variational formulations of the momentum and the continuity equations, respectively. In the current formulation, τ_{SUPG} and τ_{PSPG} are equal and are expressed as

$$\tau_{SUPG} = \tau_{PSPG} = \left[\left(\frac{2\|\boldsymbol{u}^h\|}{h} \right)^2 + \left(\frac{12\nu}{h^2} \right)^2 \right]^{-0.5}, \tag{3.6}$$

where ν is the kinematic viscosity of the fluid and h is the characteristic element length. Mittal (2000) conducted a systematic numerical study to investigate the effect of the high aspect ratio elements on the performance of the finite-element formulation for three commonly used definitions of h. In this work we use the definition based on the minimum edge length of an element.

The second series of the element level integrals are added for numerical stability at high Reynolds numbers. This is a least squares term based on the continuity equation. The stabilization parameter δ is defined as

$$\delta = \frac{h}{2} |\boldsymbol{u}^h| z, \tag{3.7}$$

with the following definition of z:

$$z = \begin{cases} \left(\frac{Re_u}{3}\right) & \text{for} \quad Re_u \leqslant 3, \\ 1 & \text{for} \quad Re_u > 3, \end{cases} \tag{3.8}$$

where Re_u is the local or element Reynolds number. More details of the finite-element formulation can be found in Tezduyar *et al.* (1992). The SUPG-based finite-element formulation has been very effectively used earlier to predict the flow past a circular cylinder, including the case of free vibrations (Singh & Mittal 2005; Kumar & Mittal 2006*a*,*b*; Prasanth *et al.* 2006).

4. Problem set-up

The circular cylinder is placed in a computational domain whose outside boundary is a rectangle (see figure 2). The origin of the Cartesian coordinate system coincides with the centre of the cylinder. The positive x_1-axis is in the downstream direction. The slip and towing tank boundary conditions associated with the present simulations are also shown in the figure. The slip boundary condition does not represent a physical situation but is very popular in the numerical community. The lateral boundaries in this case are forced to be streamlines such that the shear stress along them is zero. The towing tank boundary condition is motivated by the conditions on the lateral walls of a tow tank when a model is towed through it. For the case with no-slip sidewalls the velocity is set to zero at the lateral boundaries, and a parabolic velocity profile is specified at the inlet: $u_1 = 1 - (2\ x_2/H)^2$, $u_2 = 0$, where x_2 is the vertical distance measured from the centre of the cylinder. The Reynolds number for this flow is based on the centreline speed.

The blockage is expressed as $B = D/H$. Throughout this work, the terminology 'domain size' represents the reciprocal of the blockage, i.e. the H/D ratio. In all the simulations, the upstream and downstream boundaries are located sufficiently far from the cylinder and have no significant influence on the overall flow field. These distances are $L_u = 50D$ and $L_d = 100D$, respectively, measured from the centre of

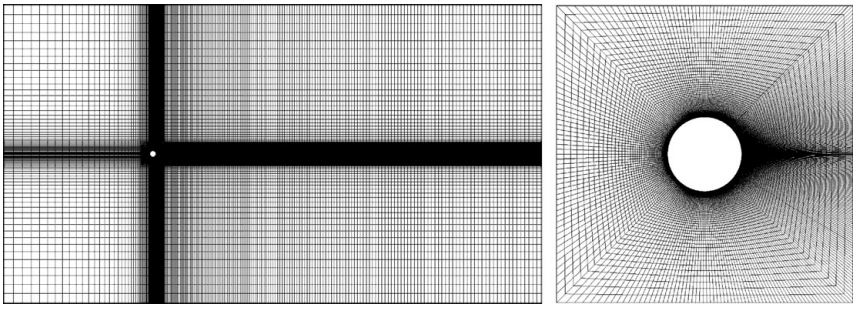

(*a*) (*b*)

FIGURE 3. Steady flow past a circular cylinder: (*a*) finite-element mesh corresponding to $B = 0.01$, consists of 93 488 nodes and 92 800 bilinear quadrilateral elements; (*b*) close-up view of the central square block containing the cylinder.

the cylinder (see § 6.2). The domain width H varies between $1.11D$ and $8000D$. This results in the blockage varying between 0.000125 and 0.90. The length and velocity scales are normalized by the cylinder radius and free-stream speed U respectively. The Reynolds number, Re $(= UD/\nu)$, is based on the cylinder diameter and free-stream speed for the slip and towing tank boundary conditions.

5. The finite-element mesh

The non-uniform finite-element mesh consisting of the bilinear quadrilateral elements and a close-up view of the mesh near the cylinder are shown in figure 3. This mesh corresponds to $B = 0.01$. The mesh is symmetric about the x_1-axis and has been constructed by combining five blocks: a central square block containing the cylinder and four neighbouring rectangular blocks located at the left, right, top and bottom of the central block. With the exception of the central block, each block consists of a Cartesian non-uniform structured mesh. The central block is constructed of non-Cartesian structured mesh made of two families of non-uniformly spaced radial and circumferential grid lines. This block is designed to have more nodes in the wake region along the circumferential direction such that the element size in the circumferential direction increases uniformly as one moves from the rear to the front portion of the cylinder. Close to the base point, the angle between two radial lines $\approx 0.18^\circ$, while the corresponding angle near the front stagnation point $\approx 1.90^\circ$. The radial thickness of the first layer of elements located on the cylinder surface h_1^r equals $0.0005D$ for all the meshes employed. Within the central block, the element size increases non-uniformly in the radial direction. The number of nodes on the cylinder surface N_t is 368 for all the meshes employed. The meshes for $B \leqslant 0.70$ contain all the five constituent blocks. For very high blockage ($B > 0.70$), only the central, left and right blocks constitute the meshes; the upper and lower blocks are dropped.

6. Validation of the method and convergence of the results

6.1. *Comparison with earlier results*

The finite-element formulation and its implementation has been validated by comparing the pressure distribution on the surface of the cylinder at $Re = 15$, 30, 36 and 40 and the total drag coefficient C_d at $Re = 40$ at very low as well as large blockages with those reported by the earlier studies. The pressure coefficient C_p

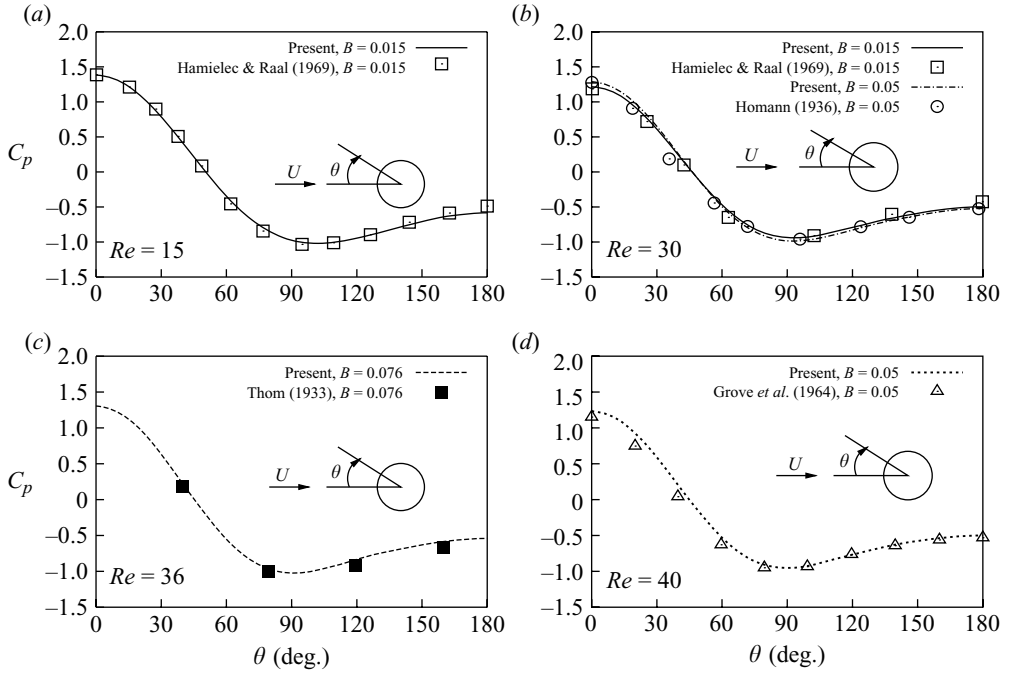

FIGURE 4. Steady flow past a circular cylinder: comparison of predicted C_p with data from literature. (*a*) C_p–θ plot at $Re = 15$; (*b*) C_p–θ plot at $Re = 30$; (*c*) C_p–θ plot at $Re = 36$; (*d*) C_p–θ plot at $Re = 40$.

computed with the slip boundary condition is shown in figure 4. As expected, the forward stagnation point is the maximum pressure point, and the corresponding pressure coefficient C_{p0} is greater than unity in all cases. For constant blockage, C_{p0} decreases with increasing Re and approaches unity, while the point of minimum pressure moves upstream, and the minimum pressure increases. This can be observed from figure 4(*a*,*b*) for $B = 0.015$.

Figure 4(*a*) compares the calculated C_p at $Re = 15$ and $B = 0.015$ with those obtained by Hamielec & Raal (1969) at the same Reynolds number and blockage. The comparison reveals excellent agreement. Figure 4(*b*) demonstrates that the predicted surface pressure distribution at $Re = 30$ is very close to the results of Hamielec & Raal (1969) for $B = 0.015$ and Homann (1936) for $B = 0.05$. Close agreement between the present results with those of Thom (1933) at $Re = 36$ is seen from figure 4(*c*). The predicted values of C_p at $Re = 40$ are compared with the experimental data of Grove *et al.* (1964) as shown in figure 4(*d*). A satisfactory match between the present and earlier results is observed.

At $Re = 40$ and $B = 0.000125$, the present calculations result in $C_{pb} = -0.4782$. Following an artificial stabilization of the wake by a splitter plate, Grove *et al.* (1964) obtained $C_{pb} = -0.45$ for the steady flow condition. They concluded that this value remains constant for $25 \leqslant Re \leqslant 177$. Fornberg (1980) estimated $C_{pb} = -0.46$ for $Re = 40$. The recent study by Posdziech & Grundmann (2007) reported $C_{pb} = -0.4736$ at $Re = 40$ and $B = 0.000125$. The values of C_d obtained from the present simulations at $B = 0.000125$ are compared with the experimental and numerical data from the literature at $Re = 40$ in table 2. For this value of low blockage, the C_d predicted using, both, the slip and towing tank boundary conditions is the same. The predicted

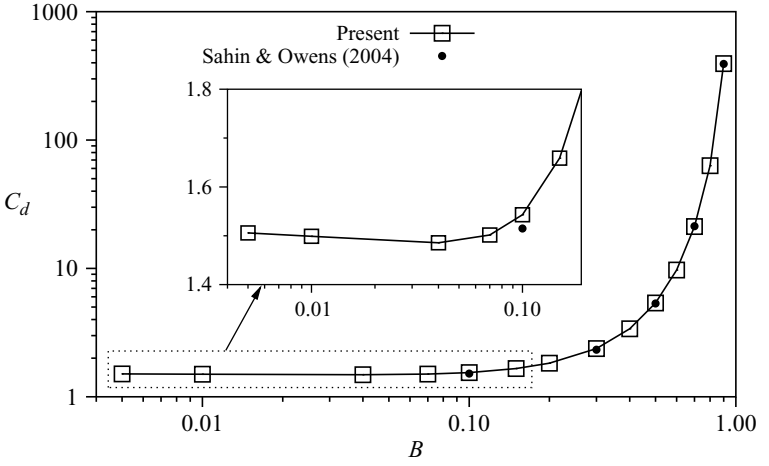

FIGURE 5. Steady flow at $Re = 40$ past a circular cylinder with no-slip sidewalls and parabolic inflow: variation of C_d with blockage. The numerical results from Sahin & Owens (2004) are also shown. The C_d axis in the inset is in the linear scale.

Studies	B	C_d
Kawaguti (1953)		1.618
Tritton (1959)		1.58
Thoman & Szewczyk (1969)		1.572
Takami & Keller (1969)	0.059	1.5359
Son & Hanratty (1969)		1.51
Dennis & Chang (1970)		1.522
Fornberg (1980)		1.4980
Henderson (1995)	0.0178	1.54
Posdziech & Grundmann (2007)	0.000125	1.4942
Present	0.000125	1.5093

TABLE 2. Steady flow at $Re = 40$ past a circular cylinder: C_d from the present study and the earlier efforts.

C_d lies in the range of the values reported by the earlier efforts. It is in very good agreement with the more recent values reported by Fornberg (1980) and Posdziech & Grundmann (2007).

For large blockages ($0.10 \leqslant B \leqslant 0.90$), C_d obtained from the present simulations using the no-slip sidewalls and those reported by Sahin & Owens (2004) at $Re = 40$ are compared in figure 5. Excellent agreement is observed for the entire range of blockage. As is shown in the inset, the present results predict a non-monotonic variation of C_d between $B = 0.005$ and $B = 0.10$.

6.2. *Streamwise extent of the domain and mesh convergence*

To study the influence of the location of the upstream and downstream boundaries on the characteristics of the flow, computations are carried out with two meshes L1 and L2 with different streamwise extents. The blockage for both the meshes is $B = 0.01$, and the spatial resolution for the two cases is kept identical.The details of the two

Mesh	L_u	L_d	Nodes	Elements
L1	$50D$	$100D$	93 488	92 800
L2	$100D$	$200D$	121 780	120 976

TABLE 3. Steady flow past a circular cylinder: details of the various meshes employed to study the effect of the streamwise location of the inflow and outflow boundaries. The other parameters for the meshes are $h_1^r = 0.001$, $N_t = 368$ and $B = 0.01$.

	L		θ_s		C_d		C_{p0}		$-C_{pb}$		
Mesh	$Re = 7$	40	7	40	7	40	7	40	7	40	Re_s
L1	0.0926	4.4995	14.62	53.63	3.3523	1.5121	1.6901	1.1626	0.7843	0.4758	6.28
L2	0.0909	4.4935	14.49	53.61	3.3428	1.5093	1.6835	1.1591	0.7832	0.4758	6.29

TABLE 4. Steady flow past a circular cylinder: effect of the streamwise location of the outflow and inflow boundaries on the characteristics of the flow. The results correspond to the slip boundary condition and $B = 0.01$.

Mesh	Nodes	Elements	h_1^r	N_t
M1	47 498	47 000	0.01	236
M2	93 488	92 800	0.001	368
M3	184 416	183 424	0.001	564

TABLE 5. Steady flow past a circular cylinder: description of the various meshes employed for the grid convergence study. The other parameters for the meshes are $L_u = 50D$, $L_d = 100D$ and $B = 0.01$.

meshes are given in table 3. The streamwise location of the upstream and downstream boundaries of mesh L2 is twice that of those of L1. The results for various Re with the two meshes are given in table 4. The difference in the L and Re_s predicted by the two meshes are 1.87 % and 0.16 %, respectively. The results from the two sets of computations for the other parameters are very similar. This demonstrates the adequacy of the streamwise extent of mesh L1. Therefore, the computations in this paper are carried out for $L_u = 50D$ and $L_d = 100D$.

To check for the grid independence, several meshes with increasing refinement are utilized to compute the $Re = 7$ and 40 flows for $B = 0.01$ blockage, using the slip boundary condition. These meshes have a streamwise extent equal to that of L1. Starting from a coarse mesh, the subsequent fine meshes are constructed by uniform global refinement. Out of the many meshes studied, table 5 lists the various parameters for meshes M1, M2 and M3. The spatial resolution increases from M1 to M3 so that the number of nodes almost doubles in each successive mesh. Mesh M2 is the same as mesh L1 described in the previous study. The results of the mesh convergence study for M1 through M3 are presented in table 6. It is found that the flow parameters for M2 and M3 are virtually identical. Based on the grid independence test shown in table 6, mesh M2 with 93 488 nodes and 92 800 elements is chosen as the reference mesh corresponding to $B = 0.01$.

The computations involving different blockages, $B \leqslant 0.20$, employ meshes that differ on the number of elements only in the upper and lower blocks (see § 5). The total numbers of nodes and elements in the central, left and right blocks have constant

	L		θ_s		C_d		C_{p0}		$-C_{pb}$		
Mesh	$Re = 7$	40	7	40	7	40	7	40	7	40	Re_s
M1	0.0924	4.4999	13.37	53.12	3.3511	1.5100	1.6922	1.1642	0.7841	0.4748	6.32
M2	0.0926	4.4995	14.62	53.63	3.3523	1.5121	1.6901	1.1626	0.7843	0.4758	6.28
M3	0.0929	4.5025	14.64	53.64	3.3519	1.5120	1.6892	1.1623	0.7847	0.4758	6.28

TABLE 6. Steady flow past a circular cylinder at $B = 0.01$, using the slip boundary condition: flow parameters for the three meshes for grid convergence study.

values of 68 768 and 68 160, respectively. The central block is a square of edge $4D$ and contains 29 808 nodes and 29 440 elements. For $0.30 \leqslant B \leqslant 0.80$ the central block is reduced to a square of edge length $1.25D$. It contains 24 656 nodes and 24 288 elements, while the sums of nodes and elements in the central, left and right blocks equal 91 302 and 90 512, respectively. For $B = 0.90$ the edge length of the central block further reduces to $1.11D$ and consists of 23 184 nodes and 22 816 elements. All the meshes have been designed to maintain the same mesh density for all the blockages as far as possible.

7. Results

The key non-dimensional parameters governing the steady laminar flow around a stationary circular cylinder are the Reynolds number and blockage. The results are presented for the computations for $6 \leqslant Re \leqslant 40$ and a wide range of blockage ($0.000125 \leqslant B \leqslant 0.80$) with both the slip and towing tank boundary conditions. The $Re = 40$ and $0.005 \leqslant B \leqslant 0.90$ results for the bubble parameters using the no-slip sidewalls are also shown. It is found that the results for $B = 0.005$ are devoid of the blockage effect and represent solutions for the unbounded flow.

The element level matrix and vector entries have been computed by employing the 2 points×2 points Gauss–Legendre quadrature formula. All the computations are carried out on a computer with AMD Opteron processor with four CPUs of 2.4 GHz clock speed. Double-precision arithmetic is used for all the calculations. The $Re = 40$ flow computed on a mesh with 93 488 nodes and 92 800 elements ($B = 0.01$) requires 582 MB of RAM and, approximately, 4 hours of CPU time when a direct solver is utilized to solve the algebraic equation system resulting from the finite element discretization. In contrast, with the matrix-free implementation of the generalized minimal residual (GMRES) method of Saad & Schultz (1986), the memory requirement reduces to a mere 34 MB, and the solution time is 1.24 hours. The dimension of the Krylov subspace is 30, and a diagonal preconditioner is employed to accelerate the convergence rate of GMRES.

7.1. *Development of the steady separation bubble with Re*

In order to demonstrate the growth of the steady separation bubble with Re, contours of the streamwise component of the velocity (for $6.3 \leqslant Re \leqslant 6.5$) and streamfunction (for $6.3 \leqslant Re \leqslant 40$) in the wake are presented in figure 6. The results in these figures are for $B = 0.01$ and the slip boundary condition. The calculations show that the separation bubble first appears at $Re = 6.28$. At $Re = 6.3$, the bubble length is of the order of the element thickness on the cylinder surface in the radial direction. As expected, the contours of ψ are symmetric about the x_1-axis. The enlargement of the separation bubble with increasing Re is clearly seen from these images. The

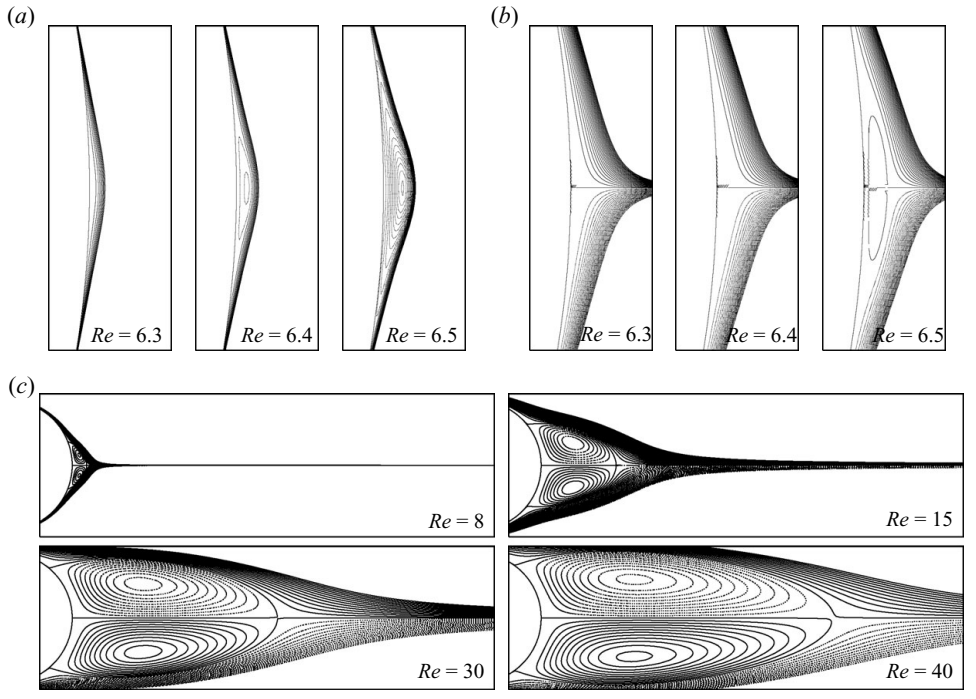

FIGURE 6. Steady flow past a circular cylinder at $B = 0.01$ and using the slip boundary condition: (*a*) $Re =$ 6.3–6.5, u_1 contours, (*b*) $Re =$ 6.3–6.5, ψ contours and (*c*) $Re = 8 - 40$, ψ contours, showing the development of the separation bubble with Re.

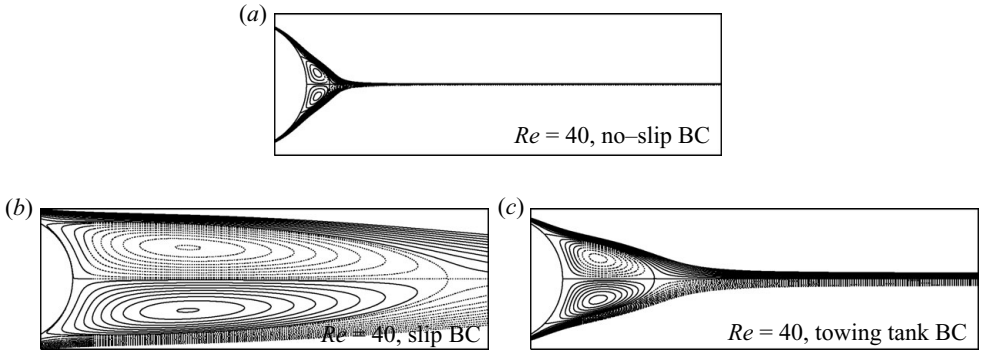

FIGURE 7. Steady flow at $Re = 40$ past a circular cylinder at $B = 0.80$, using the (*a*) no-slip, (*b*) slip and (*c*) towing tank boundary conditions: contours of ψ for the separation bubble.

separation bubble for large blockage ($B = 0.80$) is shown in figure 7 for the $Re = 40$ flow with various boundary conditions. The very significant effect of the boundary conditions on the length of the eddies for high blockage is evident from this figure.

7.2. *Variation of L and θ_s with Re*

Figure 8 shows the variation of the bubble length with Re for $B = 0.04$, 0.11 and 0.20. The results have been computed with the towing tank boundary condition. The value of L is estimated by locating the point along the wake centreline at which u_1 goes to zero. For constant blockage, it is observed that the bubble elongates approximately

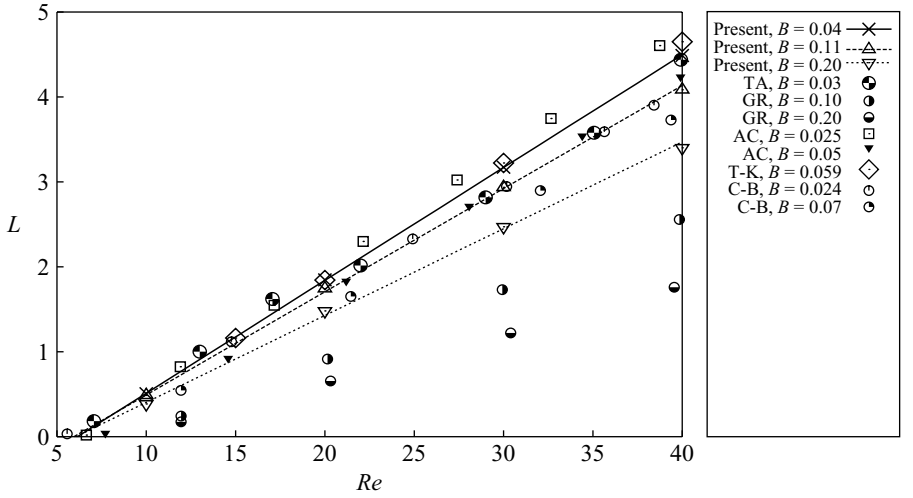

FIGURE 8. Steady flow past a circular cylinder, using the towing tank boundary condition for $Re = 6.5$–40: comparison of the bubble length, L, with the experimental and numerical data from the literature. The abbreviations used are TA, Taneda (1956); GR, Grove *et al.* (1964); AC, Acrivos *et al.* (1968); T-K, Takami & Keller (1969); C-B, Coutanceau & Bouard (1977).

linearly with Re. This is in agreement with the earlier observations. The best linear fit, using the least squares approximation, is also shown in the figure. The best linear fits for $B = 0.000125$, 0.005, 0.01 and 0.04 overlap, and for clarity only the $B = 0.04$ case is shown. The linearity of L with Re is utilized in this work to determine Re_s for each value of blockage (see § 7.4). Except at $Re = 40$, the predicted eddy length at $B = 0.04$ exhibits satisfactory agreement with those from Takami & Keller (1969) at $B = 0.059$. The data from Taneda (1956) for $B = 0.03$, Acrivos *et al.* (1968) for $B = 0.05$ and Coutanceau & Bouard (1977) for $B = 0.024$ and 0.07 lie within our data spectrum for the range of $B = 0.04$–0.20. For $B = 0.025$, Acrivos *et al.* (1968) predicted larger bubble compared to the present predictions. The eddy lengths from the study by Grove *et al.* (1964) for $B = 0.10$ and 0.20 are quite different from the ones predicted by everyone else. It is found that both the slip and towing tank boundary conditions for $0.000125 \leqslant B \leqslant 0.80$ lead to linear variation of the eddy length with Re.

The slope of the L–Re profiles obtained by using the slip and towing tank boundary conditions are listed in table 7. It is seen that both the boundary conditions result in nearly the same slope for $0.000125 \leqslant B \leqslant 0.04$. The effect of the blockage becomes important for $B > 0.04$. The difference in the slope obtained by using the slip and towing tank boundary conditions increases with increasing blockage. Also, a key observation is that using the slip boundary condition the slope decreases up to $B = 0.30$ and then increases. In contrast, the towing tank boundary condition predicts monotonic decrease of the slope with increasing B.

The least squares fit for the L–Re relationship provides the following empirical equation for the prediction of the bubble length concerning the unbounded flow ($B = 0.005$):

$$L = -0.847 + 0.1336\ Re \quad \text{for } Re_s < Re \leqslant 40. \tag{7.1}$$

The root mean square (r.m.s.) error in the curve fit ≈ 0.0002. In comparison, Sobey (2000) has proposed the following empirical equation for the bubble length in the

B	Slope of L versus Re with the slip boundary condition	Slope of L versus Re with the towing tank boundary condition
0.000125	0.1336	0.1336
0.005	0.1336	0.1336
0.01	0.1336	0.1336
0.04	0.1331	0.1328
0.07	0.1304	0.1291
0.11	0.1245	0.1214
0.15	0.1179	0.1128
0.20	0.1105	0.1022
0.30	0.1019	0.0909
0.40	0.1051	0.0852
0.50	0.1214	0.0787
0.60	0.1432	0.0705
0.70	0.1595	0.0619
0.80	0.1711	0.0539

TABLE 7. Steady flow past a circular cylinder: comparison of the slope of L–Re profiles obtained by using the slip and towing tank boundary conditions between $B = 0.000125$ and $B = 0.80$.

steady unbounded flow:

$$L = -0.506 + 0.115\ Re. \tag{7.2}$$

For the steady flow, the separation points can be identified by the vanishing of the vorticity and shear stress on the cylinder surface. We have checked, from our implementations, both methods result in identical values of the separation angle. Figure 9 shows the variation of θ_s with Re for various blockages, using the towing tank boundary condition. It is observed that θ_s increases with increasing Re. However, the variation is not linear. A steep rise in θ_s with Re is observed at the onset of the separation, and then the increase is much smaller. For $B \leqslant 0.11$, the θ_s–Re plots are virtually identical, implying minor influence of B on θ_s. However, beyond $B = 0.11$, θ_s decreases with increasing B for each Re. The predicted θ_s at low blockage match very well with the numerical data of Takami & Keller (1969) and those obtained from the empirical equation proposed by Wu *et al.* (2004). The present predictions of θ_s for $Re \geqslant 20$ are also very close to those of Coutanceau & Bouard (1977) at the blockage of 0.07. A few discrepancies with the data points of Thom (1933) for $B = 0.10$, Homann (1936) for $B = 0.10$ and Coutanceau & Bouard (1977) for $B = 0.12$ are observed.

Wu *et al.* (2004) proposed the following empirical equation for the determination of θ_s:

$$\theta_s = 78.5 - 155.2\ Re^{-0.5} \quad \text{for } 10 \leqslant Re \leqslant 200. \tag{7.3}$$

Figure 10 shows the variation of θ_s with $Re^{-0.5}$ for $10 \leqslant Re \leqslant 40$ and $0.005 \leqslant B \leqslant 0.20$ for the present data. It is observed that for both types of boundary conditions, these profiles are linear for all blockages. Further, they are virtually identical for $B \leqslant 0.11$. The empirical equation for θ_s for the unbounded flow obtained by the least squares curve fit is

$$\theta_s = 77.66 - 152.65\ Re^{-0.5} \quad \text{for } 10 \leqslant Re \leqslant 40. \tag{7.4}$$

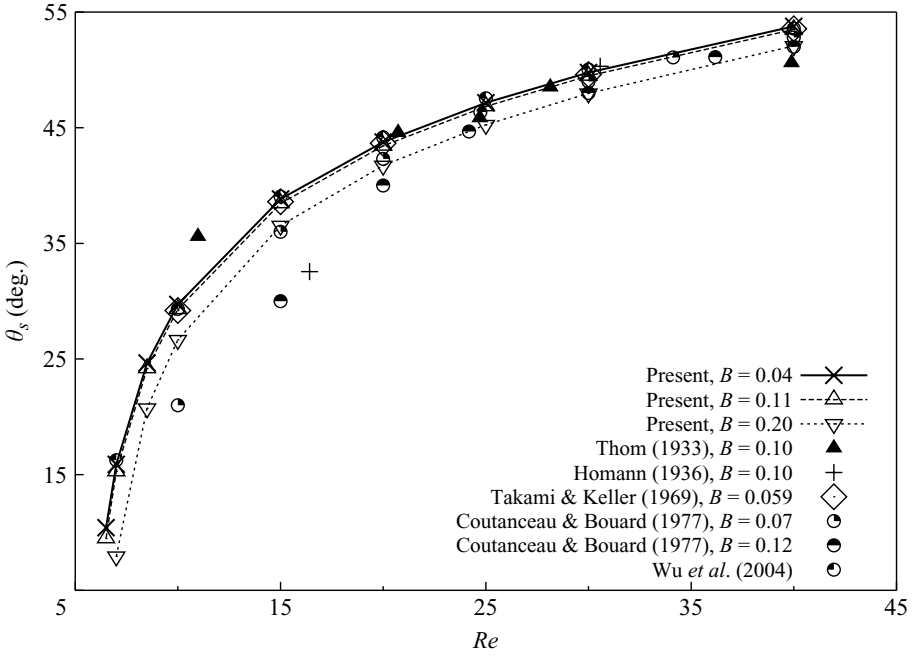

FIGURE 9. Steady flow past a circular cylinder, using the towing tank boundary condition for $Re = 6.5$–40: comparison of the separation angle, θ_s, with the experimental and numerical data from the literature.

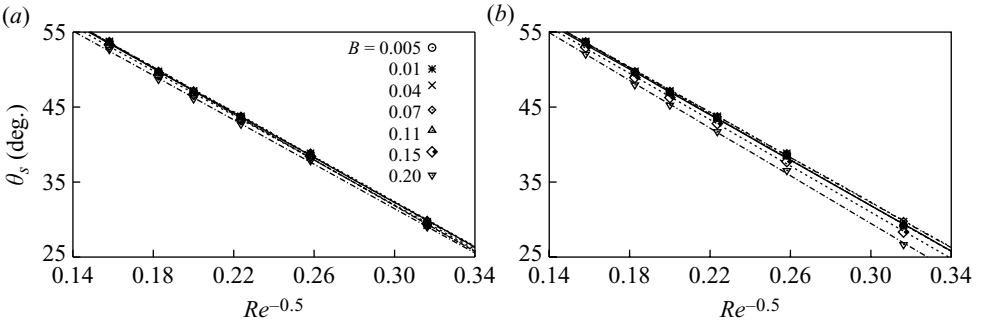

FIGURE 10. Steady flow past a circular cylinder: variation of θ_s with $Re^{-0.5}$ for $10 \leqslant Re \leqslant 40$ and $0.005 \leqslant B \leqslant 0.20$ for the (*a*) slip and (*b*) towing tank boundary conditions.

The associated r.m.s. error for this fit is 0.04. This equation is in very good agreement with (7.3) proposed by Wu *et al.* (2004).

The L–Re and θ_s–Re curves for the unbounded flow ($B = 0$), obtained via the least squares curve fit, are shown in figure 11. The data points for the curve fit are determined via Richardson's extrapolation of order two. The computed results for $B = 0.005$ and 0.01 are utilized for this purpose. The empirical equations thus obtained are given by

$$L = -0.848 + 0.1336\ Re \quad \text{for } Re_s < Re \leqslant 40, \tag{7.5}$$

$$\theta_s = 77.66 - 152.70\ Re^{-0.5} \quad \text{for } 10 \leqslant Re \leqslant 40 \tag{7.6}$$

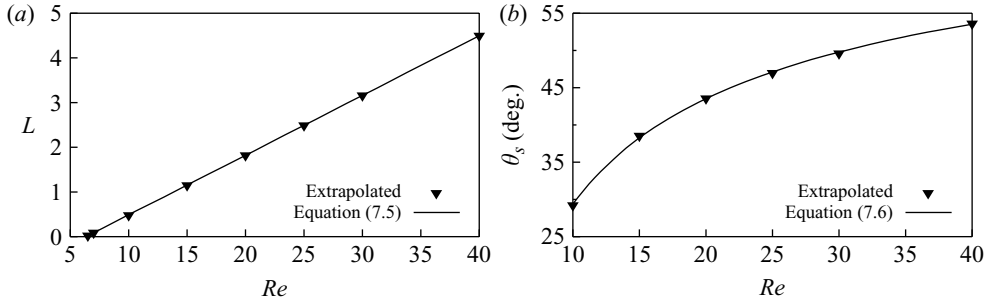

FIGURE 11. Steady flow past a circular cylinder: (*a*) *L*–*Re* and (*b*) θ_s–*Re* curves for the unbounded flow ($B = 0$) obtained by fitting the extrapolated data.

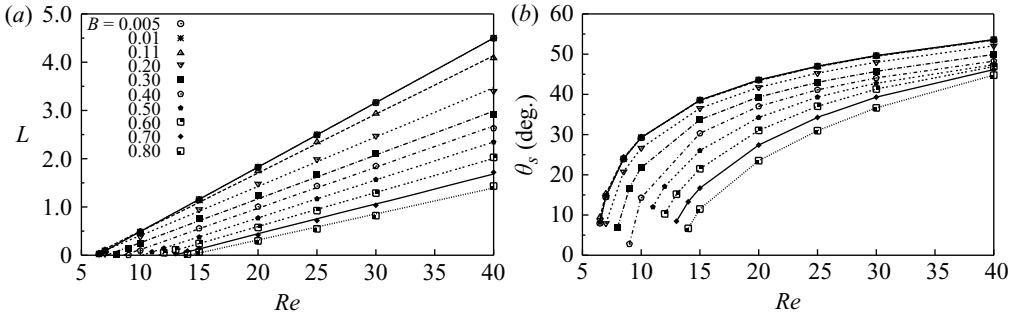

FIGURE 12. Steady flow past a circular cylinder, using the towing tank boundary condition for $0.005 \leqslant B \leqslant 0.80$: variation of the (*a*) bubble length and (*b*) separation angle with *Re*.

These equations are very similar to (7.1) and (7.4) obtained via curve fit through the computed results. The variation of L and θ_s with Re, for the range of blockage studied in this effort, is shown in figure 12.

7.3. *Effect of the blockage and boundary conditions on L and* θ_s

The variation of L and θ_s with the blockage has been investigated for $0.005 \leqslant B \leqslant 0.80$ for both the slip and towing tank boundary conditions. The results are presented in figure 13 for $Re = 7$, 20, 30 and 40. For $B \leqslant 0.01$, L and θ_s are free from the blockage effect. Between $B = 0.01$ and $B = 0.15$, a non-monotonic variation of L and θ_s with B is observed. We refer to this behaviour as the first non-monotonic variation. The values of L and θ_s increase with the blockage for small values of B and then decrease. The blockage at which L and θ_s achieve the maximum values is a function of Re and the boundary condition. We refer to this value as the critical blockage. For instance at $Re = 7$ the maximum is achieved at $B = 0.07$ and 0.11 with the towing tank and slip boundary conditions, respectively. As Re increases, the critical blockage decreases. Fornberg (1991) investigated the steady wake for flow past a cylinder for $Re \leqslant 800$. Even though it was not explicitly pointed out, careful observation of figure 11 in his paper shows non-monotonic variation of the bubble length with the blockage. For $0.01 \leqslant B \leqslant 0.04$, the slip and towing tank boundary conditions predict identical increase of L and θ_s for all Re considered. For all blockages beyond $B = 0.04$, L and θ_s obtained with the slip boundary condition are higher than those obtained with the towing tank boundary condition. In general, for large B compared to the towing tank boundary condition, slip boundary condition results in values that are closer to the ones for the unbounded flow (for $B = 0.005$). For $B > 0.15$, the towing tank

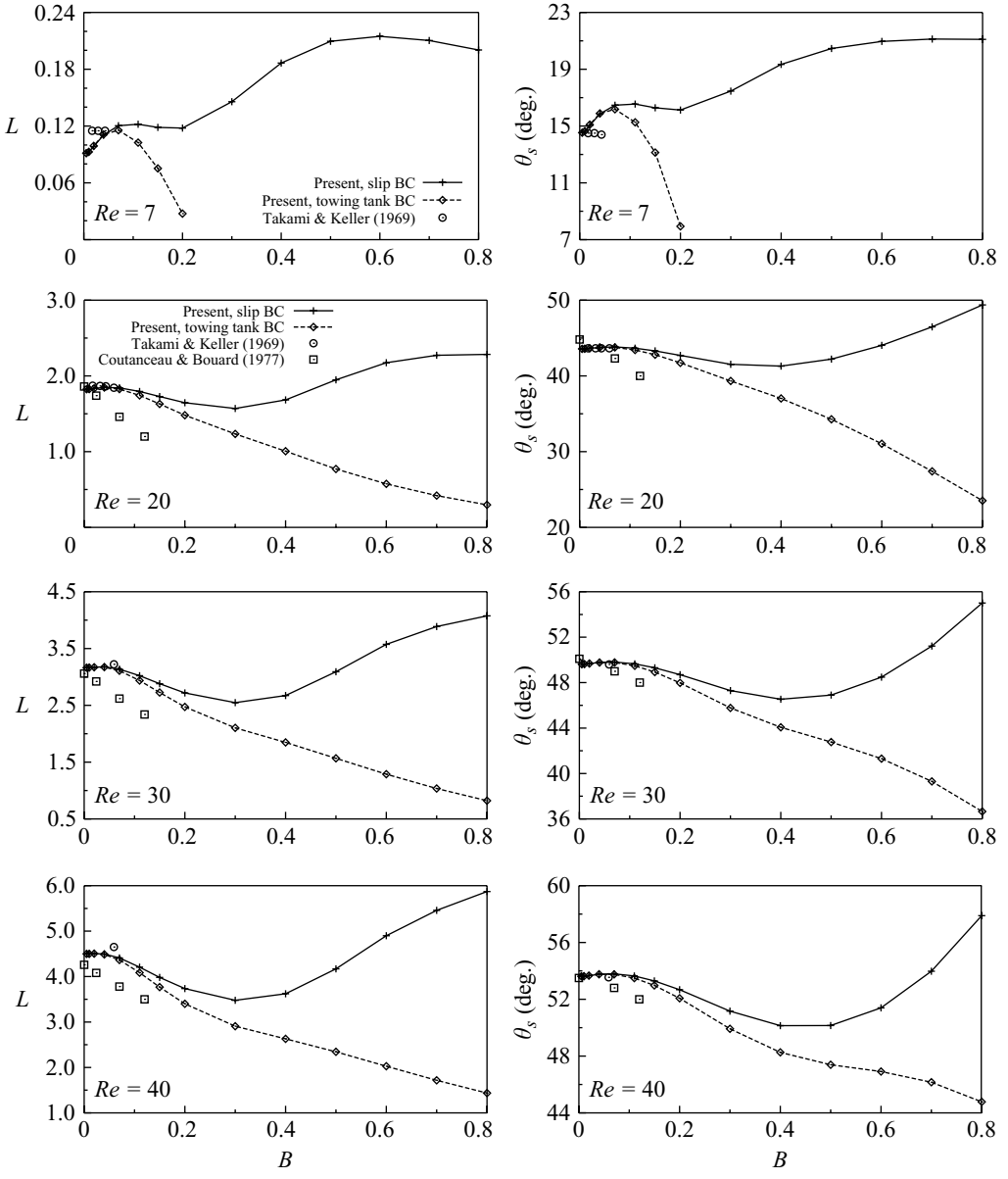

FIGURE 13. Steady flow past a circular cylinder for $7 \leqslant Re \leqslant 40$ and $0.005 \leqslant B \leqslant 0.80$: variation of L and θ_s with B. Also shown are the results from the earlier studies. BC: boundary condition.

boundary condition predicts monotonic decrease of L and θ_s for all Re. However, the slip boundary condition leads to a much more complex variation that depends on Re. For $Re \geqslant 30$ and $B \geqslant 0.30$, L and θ_s are found to increase with B leading to a second regime of non-monotonicity. At very low Re, say $Re = 7$, the second regime of non-monotonicity occurs at relatively low blockage. Also, a regime of third non-monotonicity is observed for large blockage in the variation of eddy length with B.

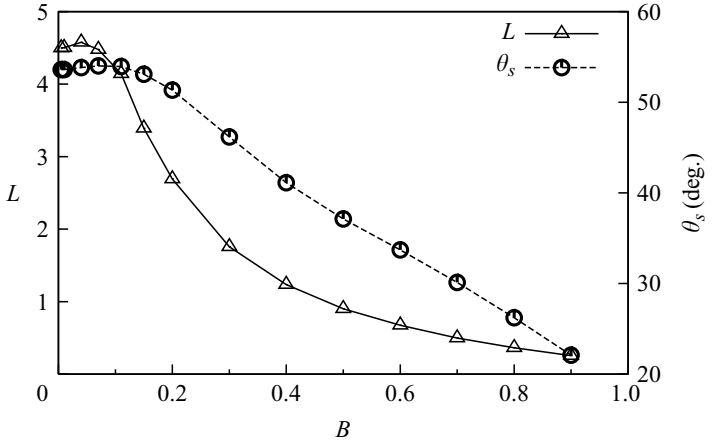

FIGURE 14. $Re = 40$ steady flow past a circular cylinder for $0.005 \leqslant B \leqslant 0.90$ using the no-slip sidewalls: variation of L and θ_s with B.

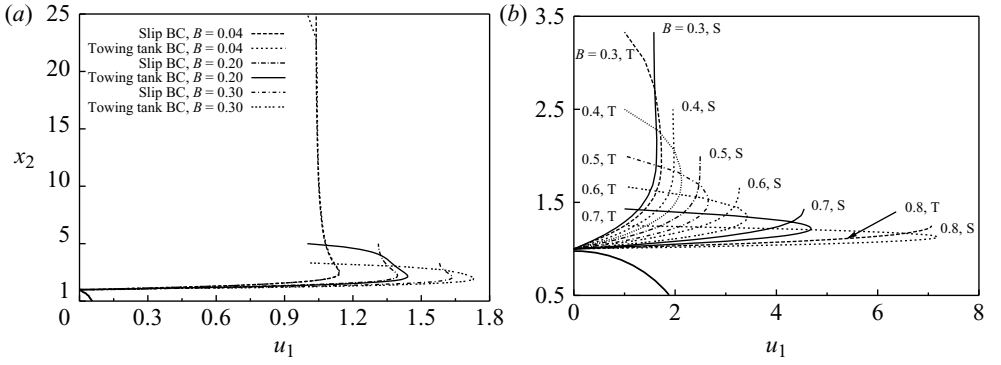

FIGURE 15. Steady flow at $Re = 20$ past a circular cylinder: variation of the x_1 component of velocity with x_2 at $x_1 = 0$ for the slip and towing tank boundary conditions for (*a*) $0.04 \leqslant B \leqslant 0.30$ and (*b*) $0.30 \leqslant B \leqslant 0.80$. The surface of the cylinder is shown in solid line. In (*b*), S and T denote the slip and towing tank boundary conditions, respectively. BC: boundary condition.

At $Re = 20$ and 30, a satisfactory match is found with the results of Takami & Keller (1969) for $B < 0.07$. However, significant discrepancies are found with the results of Coutanceau & Bouard (1977) for relatively higher blockage. In the experiments of Coutanceau & Bouard (1977) the blockage, B, is based on the diameter of the tank. In the present computations, the outer domain is a rectangle. With respect to the present definition of the blockage, the effective blockage in the experiments of Coutanceau & Bouard (1977) is, therefore, higher than what they report. This, then, might explain the discrepancies between their results and the present results.

The variation of L and θ_s with B at $Re = 40$ using the no-slip sidewalls is shown in figure 14. The variation is similar to that for the towing tank boundary condition, i.e. non-monotonicity at low blockage, and decrease in the bubble parameters with increasing B. Figure 15 shows the cross-flow variation of the streamwise component of the velocity at $x_1 = 0$ for the $Re = 20$ flow at low as well as high blockages for the two types of boundary conditions. Compared to the unbounded flow, for $B \geqslant 0.20$, the presence of the lateral walls leads to an overall acceleration of the flow. The

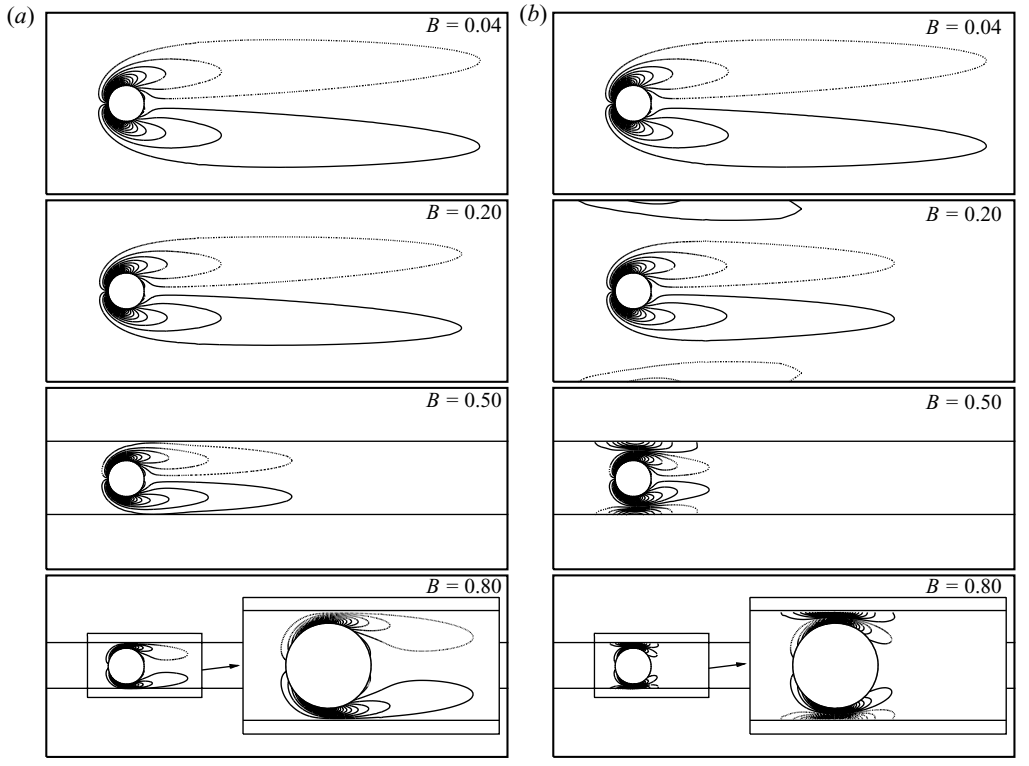

FIGURE 16. Steady flow at $Re = 20$ past a circular cylinder: vorticity fields obtained with the (a) slip and (b) towing tank boundary conditions for $0.04 \leqslant B \leqslant 0.80$. The broken lines denote negative while the solid lines represent positive values of the vorticity. For $B = 0.50$ and 0.80, the horizontal lines near the cylinder represent the sidewalls.

specification of the free-stream speed at the lateral walls for flow in the towing tank boundary condition leads to an additional flow acceleration. For low blockage ($B = 0.04$), the slip and towing tank boundary conditions lead to virtually the same velocity profiles. However, for $B \geqslant 0.20$ the towing tank boundary condition leads to significantly larger acceleration as seen in figure 15. This results in delayed flow separation for the towing tank boundary condition and therefore a shorter bubble.

To further investigate the effect of the blockage and boundary conditions, we study the vorticity fields of the $Re = 20$ flow for certain values of B. The vorticity fields for the slip and towing tank boundary conditions are shown in figure 16, while figure 17 shows the vorticity distribution on the cylinder surface. For low blockage ($B = 0.04$) the vorticity fields obtained with both the boundary conditions are virtually identical. However, for $B \geqslant 0.20$ the vorticity is generated at the sidewalls due to the imposition of the free-stream speed for the towing tank boundary condition (figure 16b). The strength of the wall-generated vorticity increases with increasing blockage. This interferes with the advection of the vorticity generated on the surface of the cylinder and leads to the delay of flow separation. This is reflected by the downstream movement of the zero-vorticity point as seen from the inset of figure 17(b). In contrast, the slip boundary condition results in very similar vorticity fields for $B = 0.04$ and 0.20 (figure 16a). For $B \geqslant 0.50$, the shortening of the streamwise extent of the vorticity contours is associated with the upstream movement of the zero-vorticity point. The

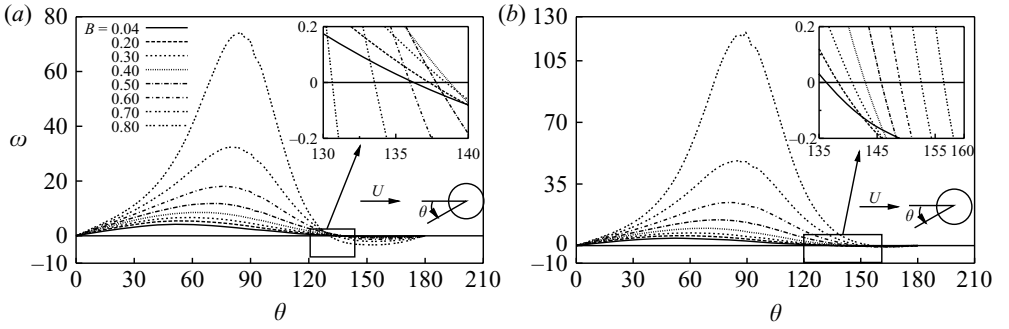

FIGURE 17. Steady flow at $Re = 20$ past a circular cylinder: vorticity distribution on the cylinder surface for $0.04 \leqslant B \leqslant 0.80$, using the (*a*) slip and (*b*) towing tank boundary conditions.

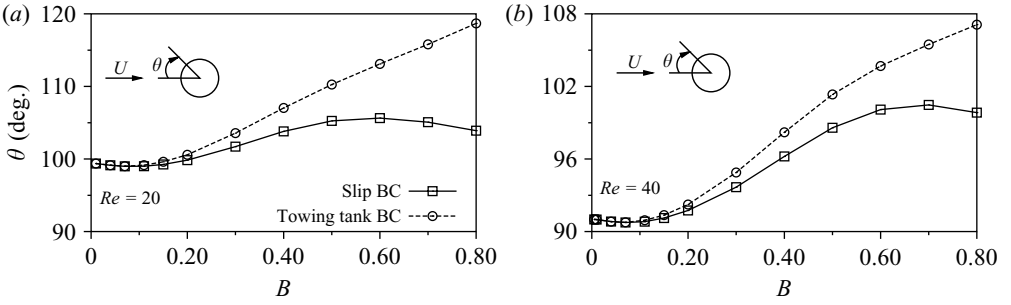

FIGURE 18. Steady flow past a circular cylinder for $0.005 \leqslant B \leqslant 0.80$: variation with B of the location at which $\partial C_p/\partial\theta = 0.05$ is achieved for (*a*) $Re = 20$ and (*b*) $Re = 40$. BC: boundary condition.

reversal of the movement of the zero-vorticity point for $B \geqslant 0.50$ is clearly seen from the inset of figure 17(*a*). The location of the zero-vorticity point is a measure of the separation angle (see § 7.2).

The adverse pressure gradient plays a major role in the flow separation. To investigate the possible cause of the non-monotonic variation of L and θ_s with the blockage, we study the adverse pressure gradient on the surface of the cylinder. Figure 18 shows, for various blockages, the location on the cylinder surface at which a pressure gradient corresponding to $\partial C_p/\partial\theta = 0.05$ occur. Two representative Reynolds numbers are chosen: $Re = 20$ and 40. For both Re it is seen that the locations corresponding to $\partial C_p/\partial\theta = 0.05$ show non-monotonic variation with B. This, therefore, leads to non-monotonic variation of L and θ_s with the blockage.

7.4. *Re_s for the confined and unbounded flow*

It was shown in § 7.2 (figure 8) that the eddy length varies linearly with Re. We utilize this variation to estimate Re_s for each blockage. Figure 19 shows the variation of Re_s with H/D $(= 1/B)$ for the slip as well as towing tank boundary conditions. The variation of Re_s with H/D for the two boundary conditions is quite different for $H/D < 25$, i.e. $B > 0.04$. While both the boundary conditions result in a non-monotonic variation of Re_s with H/D, the towing tank boundary condition predicts higher values of Re_s. This can be clearly seen in figure 19. The present results with the towing tank boundary condition predict a decrease in Re_s with H/D for $H/D < 14.28$ and an increase thereafter. This is the first time that the non-monotonic variation of

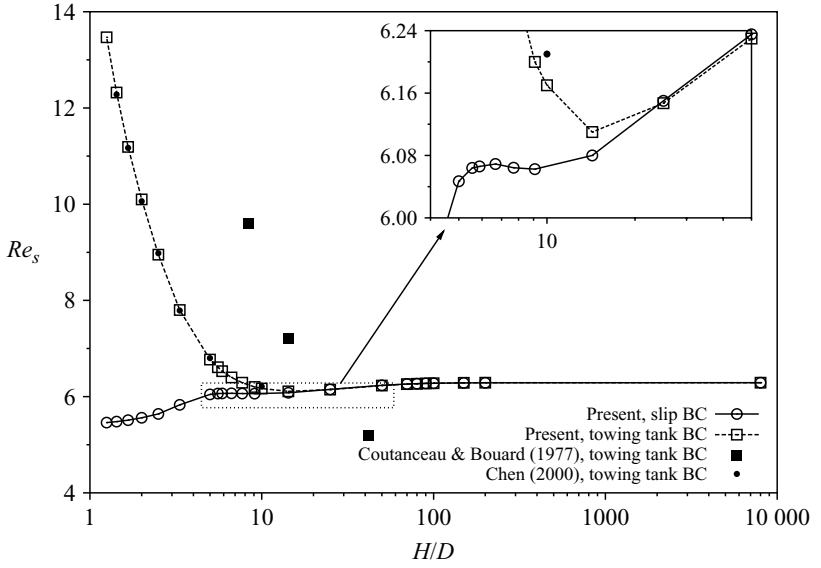

FIGURE 19. Domain size dependence of Re_s, using the slip and towing tank boundary conditions for steady flow past a circular cylinder for $1.25 \leqslant H/D \leqslant 8000$, i.e. $0.000125 \leqslant B \leqslant 0.80$. Shown in the inset are the non-monotonic regimes associated with both the boundary conditions. BC: boundary condition.

Re_s with the domain size is being reported. Also shown in figure 19 is the comparison of the present predictions using the towing tank boundary condition with those of Coutanceau & Bouard (1977) and Chen (2000). The present results show considerable divergence with those of Coutanceau & Bouard (1977) but display excellent agreement with the more recent results of Chen (2000) for $1.43 \leqslant H/D \leqslant 10$, i.e. $0.10 \leqslant B \leqslant 0.70$. The discrepancies with Coutanceau & Bouard (1977) seem to stem from the different definition of the blockage used in the two cases (see § 7.3).

The effect of the boundary conditions, on prediction of Re_s, is insignificant for $H/D \geqslant 25$ ($B \leqslant 0.04$). The blockage effect becomes negligible for $B \leqslant 0.01$. Figure 19 can be utilized to estimate Re_s for the unbounded flow. It is found to be $Re_s \approx 6.29$. Richardson's extrapolation of order two and the values of Re_s at $B = 0.005$ and 0.01 are utilized to predict Re_s for the unbounded flow ($B = 0$). This method also results in $Re_s \approx 6.29$. From table 1 it is seen that this value is close to the prediction of Dennis & Chang (1970). Another observation that can be made from figure 19 is that for high blockage ($H/D < 5.88$), compared to the towing tank boundary condition, the slip boundary condition predicts Re_s that is closer to that for the unbounded flow.

Srinivasan (2006) suggested an analytical criterion to determine Re_s for the flow past a circular cylinder from the velocity field. It was shown that for $Re = Re_s$, $\partial^2 u_1/\partial x_1^2$ approaches zero at the base/rear stagnation point. Figure 20 shows the variation of $\partial^2 u_1/\partial x_1^2$ at the base point of the cylinder for various Re and B. As shown by Srinivasan (2006), a linear variation of $\partial^2 u_1/\partial x_1^2$ with Re is observed for all B and both the boundary conditions.

Listed in table 8 is the prediction of Re_s for various B and boundary conditions from the vanishing of $\partial^2 u_1/\partial x_1^2$ and the eddy length, L. Very good agreement between the predictions from the two criteria is observed. Furthermore, the non-monotonic variation of Re_s with B is exhibited by both the predictions. Overall, the maximum difference between the two sets of predictions is less than 1 %.

	Slip boundary condition		Towing tank boundary condition	
B	$Re_s(L)$	$Re_s(\partial^2 u_1/\partial x_1^2)$	$Re_s(L)$	$Re_s(\partial^2 u_1/\partial x_1^2)$
0.000125	6.29	6.31	6.29	6.31
0.005	6.29	6.31	6.29	6.31
0.0066	6.29	6.31	6.29	6.31
0.01	6.28	6.30	6.28	6.30
0.04	6.15	6.17	6.15	6.17
0.07	6.08	6.10	6.11	6.13
0.11	6.06	6.08	6.20	6.22
0.15	6.07	6.09	6.40	6.43
0.20	6.05	6.07	6.77	6.80
0.30	5.83	5.87	7.80	7.83
0.40	5.64	5.69	8.95	8.98
0.50	5.56	5.59	10.10	10.12
0.60	5.51	5.53	11.19	11.22
0.70	5.48	5.49	12.32	12.37
0.80	5.46	5.46	13.47	13.53

TABLE 8. Steady flow past a circular cylinder for $0.000125 \leqslant B \leqslant 0.80$: Re_s obtained for various B and the slip and towing tank boundary conditions; $Re_s(L)$ and $Re_s(\partial^2 u_1/\partial x_1^2)$ represent the separation Reynolds numbers obtained using the eddy length and $\partial^2 u_1/\partial x_1^2 = 0$ criteria, respectively.

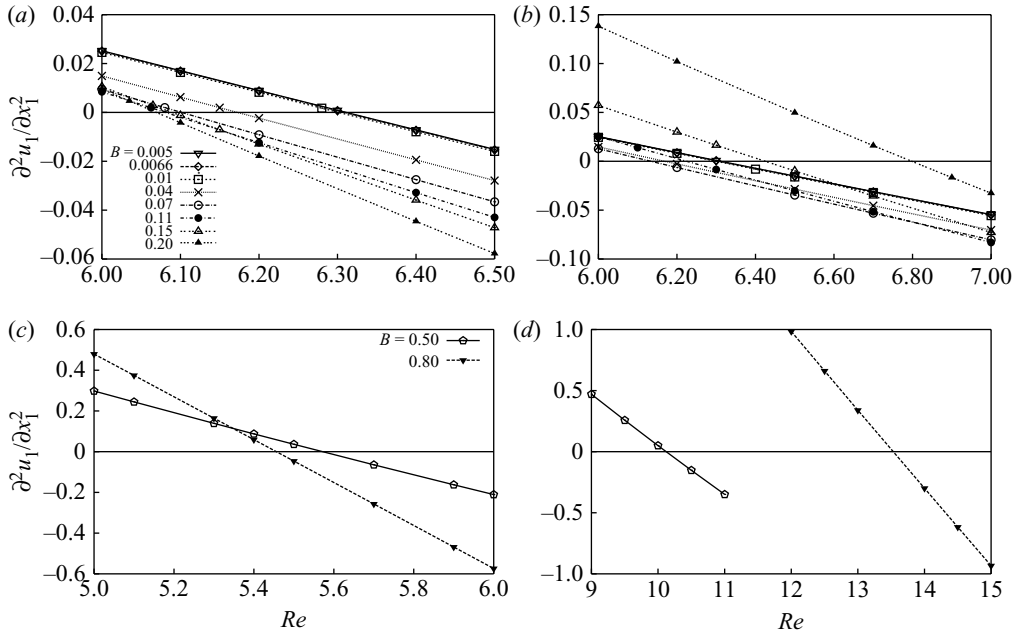

FIGURE 20. Steady flow past a circular cylinder: variation of $\partial^2 u_1/\partial x_1^2$ at the base point with Re for various B with the (a), (c) slip and (b), (d) towing tank boundary conditions.

7.5. *Effect of the blockage and boundary conditions on C_d and $-C_{pb}$*

Figure 21 shows the variation of C_d with the domain size for $Re = 10$, 20 and 40. At each blockage, compared to the slip, towing tank boundary condition results in

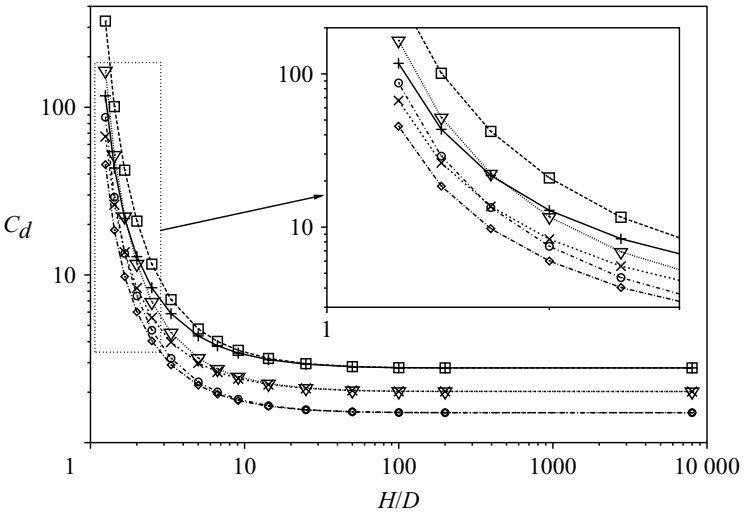

FIGURE 21. Steady flow past a circular cylinder for $1.25 \leqslant H/D \leqslant 8000$: variation of C_d with the domain size for various Re. For the slip boundary condition: +, $Re = 10$; ×, $Re = 20$; ◇, $Re = 40$. For the towing tank boundary condition: □, $Re = 10$; ▽, $Re = 20$; ○, $Re = 40$.

a higher value. With increasing B, C_d displays rapid and monotonic increase. The sensitivity to the boundary conditions disappears for $B < 0.04$. The effect of the blockage is found to be negligible for $B \leqslant 0.01$. The asymptotic variation of C_d with H/D can be utilized to estimate the value for the unbounded flow. Unlike the no-slip sidewalls (see figure 5), the slip and towing tank boundary conditions do not predict any non-monotonicity of C_d with B at low B.

Figure 22 depicts the variation of the base suction, $-C_{pb}$, with the domain size for various Re and boundary conditions. As is seen for C_d, the variation of $-C_{pb}$ is independent of the blockage for $B \leqslant 0.01$. For $H/D < 100$, $-C_{pb}$ predicted by the slip boundary condition exceeds the corresponding prediction by the towing tank boundary condition for all Re considered. With increasing domain size, the slip boundary condition predicts a monotonic decrease in $-C_{pb}$ for all Re. In contrast, the towing tank boundary condition predicts a non-monotonic variation of $-C_{pb}$ with H/D at $Re = 10$ and 20. A monotonic decrease in $-C_{pb}$ with H/D is observed at $Re = 40$. For a given domain size, the slip boundary condition predicts a monotonic decrease in $-C_{pb}$ for $H/D \geqslant 5$ and a monotonic increase for $H/D \leqslant 2$ with increasing Re. In contrast, a non-monotonic variation of $-C_{pb}$ with Re is observed with the towing tank boundary condition for $H/D \leqslant 5$.

7.6. *Variation of the parameters with Re*

The variation of C_d and $-C_{pb}$ with Re for $B = 0.01$ are compared with the results of Henderson (1995) and Posdziech & Grundmann (2007) in figure 23. The blockage $B = 0.01$ is low enough to give results for the unbounded flow. In addition, it is found that at $B = 0.01$ the results are independent of the boundary conditions. It is seen that the present results are in very good agreement with those of Posdziech & Grundmann (2007). Discrepancies are observed with the results from Henderson (1995) for $-C_{pb}$ variation, while surprisingly, the C_d values are in very good agreement.

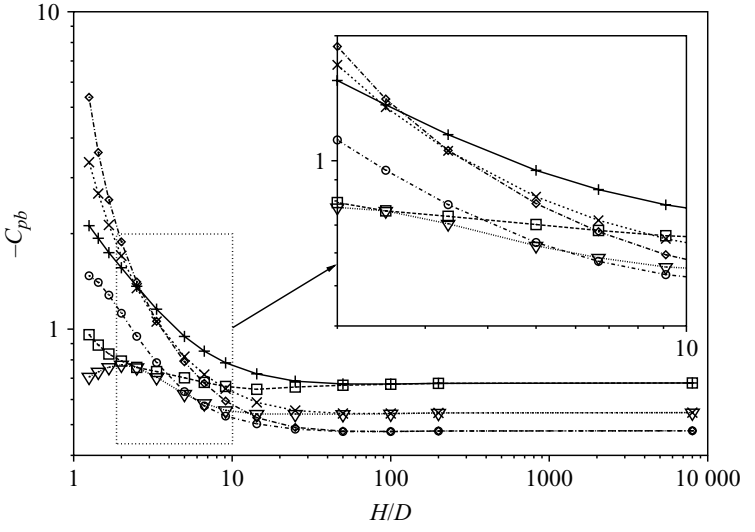

FIGURE 22. Steady flow past a circular cylinder for $1.25 \leqslant H/D \leqslant 8000$: variation of $-C_{pb}$ with the domain size for various Re. For the slip boundary condition: +, $Re = 10$; ×, $Re = 20$; ⋄, $Re = 40$. For the towing tank boundary condition: □, $Re = 10$; ▽, $Re = 20$; ○, $Re = 40$.

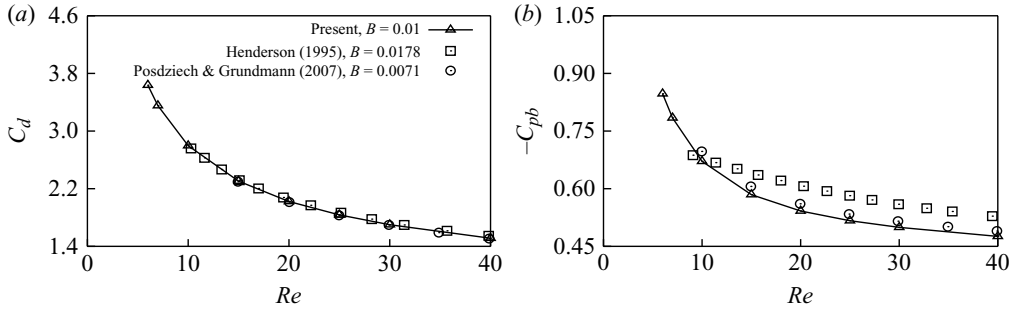

FIGURE 23. Steady flow at $B = 0.01$ past a circular cylinder: variation of (*a*) C_d and (*b*) $-C_{pb}$ with Re. Also shown are the results from Henderson (1995) and Posdziech & Grundmann (2007).

Smith (1981) proposed a C_d–Re variation for the steady flow:

$$C_d = 0.50\ (1 + 7.61\ Re^{-0.5}). \tag{7.7}$$

Following the same lead, figure 24 shows the variation of C_d with $Re^{-0.5}$ for $Re \geqslant 15$. A linear curve fit is obtained for both the boundary conditions. The curve fit for $B = 0.005$ is found to be independent of the boundary conditions and is given as

$$C_d = 0.26 + 7.89\ Re^{-0.5} \quad \text{for } 15 \leqslant Re \leqslant 40. \tag{7.8}$$

By using the least squares curve fit, empirical equations are obtained for the pressure and viscous components of C_d. For the unbounded flow, the variation of C_{dp} and C_{dv} with Re is given as

$$C_{dp} = 0.583 + 4.311\ Re^{-0.64} \quad \text{for } 6 \leqslant Re \leqslant 40, \tag{7.9}$$

$$C_{dv} = -0.016 + 4.938\ Re^{-0.60} \quad \text{for } 6 \leqslant Re \leqslant 40. \tag{7.10}$$

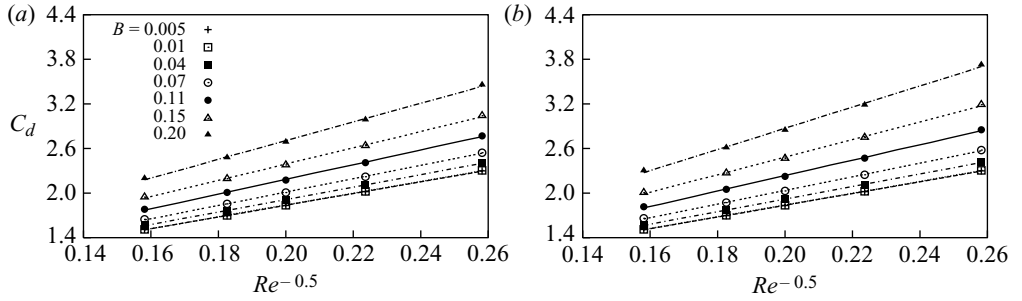

FIGURE 24. Steady flow past a circular cylinder: variation of C_d with $Re^{-0.5}$ for $15 \leqslant Re \leqslant 40$ and $0.005 \leqslant B \leqslant 0.20$ for the (a) slip and (b) towing tank boundary conditions.

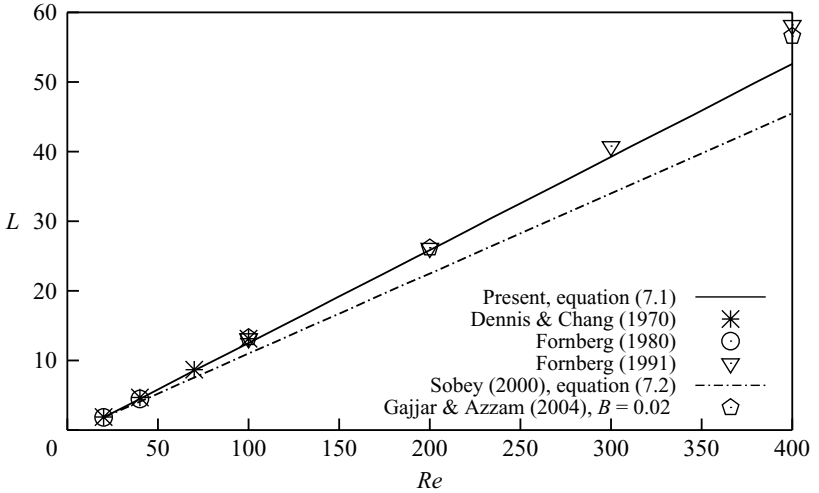

FIGURE 25. Steady flow past a circular cylinder: comparison of L extrapolated from the proposed equation (7.1) and numerical data from the literature for $20 \leqslant Re \leqslant 400$. Also plotted is the formula proposed by Sobey (2000).

The empirical equations for $-C_{pb}$ and ω_{max} corresponding to the unbounded flow, obtained via the least squares curve fit are given as

$$-C_{pb} = 0.413 + 2.627\ Re^{-1} \quad \text{for } 6 \leqslant Re \leqslant 40, \tag{7.11}$$

$$\omega_{max} = -0.2284 + 0.9430\ Re^{0.5} \quad \text{for } 6 \leqslant Re \leqslant 40. \tag{7.12}$$

7.7. *Prediction of the parameters for the steady flow at higher Re*

The empirical equations obtained for L, C_d, C_{dp}, C_{dv} and ω_{max} in the steady recirculation regime, (7.1), (7.8), (7.9), (7.10) and (7.12), are linearly extrapolated to predict these parameters for $Re > 40$ and compared with the empirical equations and numerical data from the literature.

Figure 25 compares the bubble length L extrapolated from (7.1) with the formula proposed by Sobey (2000), given by (7.2), and the numerical data from the literature for $20 \leqslant Re \leqslant 400$. It is found that the relation proposed by Sobey (2000) underpredicts the bubble length for the Re range considered. For $Re \leqslant 100$, the predicted results match well with the results of Dennis & Chang (1970). Up to $Re = 300$, L predicted by the proposed equation displays satisfactory agreement with those predicted by

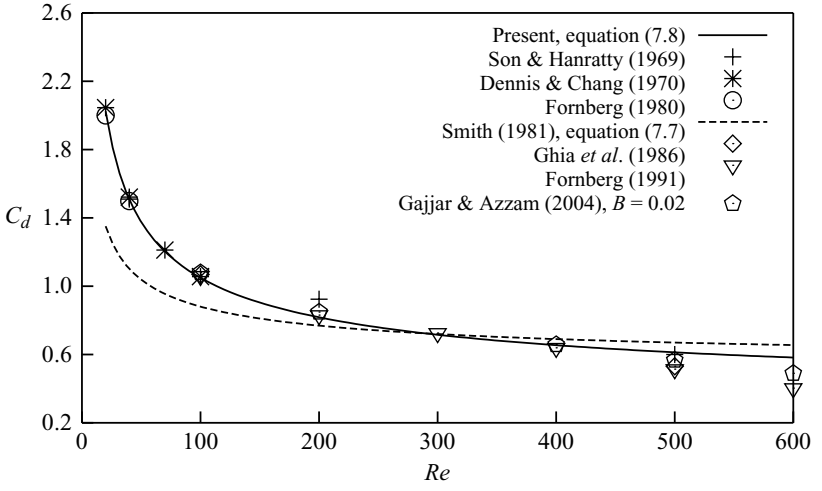

FIGURE 26. Steady flow past a circular cylinder: comparison of C_d extrapolated from the proposed equation (7.8) and numerical data from the literature for $20 \leqslant Re \leqslant 600$. Also plotted is the formula proposed by Smith (1981).

Fornberg (1980, 1991) and Gajjar & Azzam (2004). At $Re = 400$, L predicted by (7.1) is 9.62 % smaller than that predicted by Fornberg (1991) and 7.07 % shorter compared to the prediction of Gajjar & Azzam (2004).

In figure 26, the variation of C_d with Re predicted by (7.8) is compared with the formula proposed by Smith (1981) and the numerical data from the literature for the steady flow for $20 \leqslant Re \leqslant 600$. For $Re \leqslant 100$, the predicted results display close agreement with those of Son & Hanratty (1969) and Dennis & Chang (1970). For $Re \leqslant 400$, C_d predicted by the proposed equation (7.8) compares favorably with the data from Fornberg (1980, 1991), Ghia *et al.* (1986) and Gajjar & Azzam (2004). In general, the predictions with the present equation are better than (7.7) proposed by Smith (1981).

The pressure and viscous drag coefficients extrapolated from the proposed equations (7.9) and (7.10), respectively, are presented in figure 27 and also compared with various numerical results for $6 \leqslant Re \leqslant 100$. It is observed that within the Re range, C_{dp} and C_{dv} are of the same order of magnitude with C_{dp} exceeding C_{dv}. The comparison reveals a satisfactory agreement between the predicted results and the results of Dennis & Chang (1970), Henderson (1995) and Posdziech & Grundmann (2007).

The maximum vorticity on the cylinder surface extrapolated from the proposed relation given by (7.12) for $7 \leqslant Re \leqslant 400$ is compared with various numerical data from the literature as shown in figure 28. For $Re \leqslant 100$, ω_{max} predicted by (7.12) match well with the results of Dennis & Chang (1970). For $Re \leqslant 200$, the predicted ω_{max} compares favorably with the results of Fornberg (1980, 1991) and Gajjar & Azzam (2004).

8. Conclusions

A stabilized finite-element method has been employed to investigate the steady, laminar flow around a stationary circular cylinder. Two sets of boundary conditions, namely the slip and towing tank, have been studied. Results have been presented for

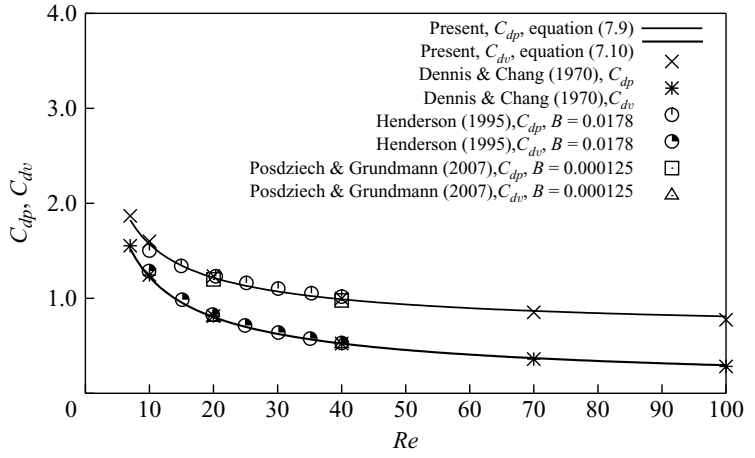

FIGURE 27. Steady flow past a circular cylinder: comparison of C_{dp} and C_{dv} extrapolated from the proposed equations (7.9) and (7.10), respectively, and numerical data from the literature for $6 \leqslant Re \leqslant 100$.

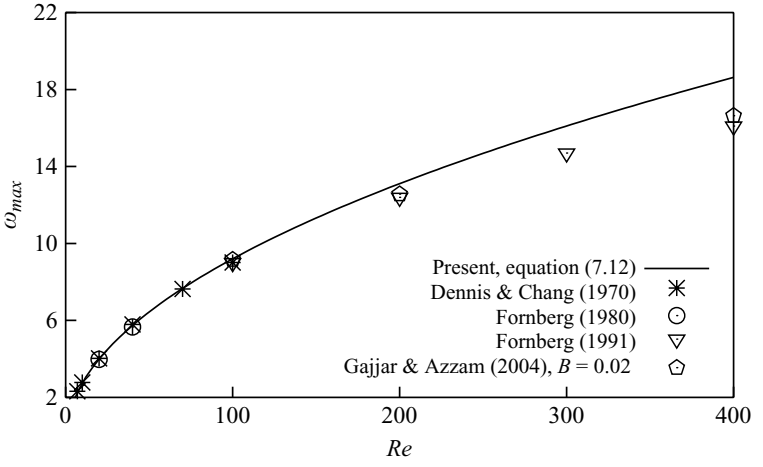

FIGURE 28. Steady flow past a circular cylinder: comparison of ω_{max} extrapolated from the proposed equation (7.12) and numerical data from the literature for $7 \leqslant Re \leqslant 400$.

$6 \leqslant Re \leqslant 40$ and $0.000125 \leqslant B \leqslant 0.80$. The results for $B = 0.005$ closely represent the unbounded flow.

Re_s from the earlier studies varies between 3.2 and 7. The critical Reynolds number for the onset of the flow separation has been found to be $Re_s \approx 6.29$ for the unbounded flow. The separation initiates from the base point, i.e. $\theta_s = 0°$, at $Re = Re_s$. The bubble length is found to vary approximately linearly with Re. Irrespective of the boundary conditions and blockage, the steady flow displays symmetry about the x_1-axis.

For the first time, it is found that θ_s and Re_s display non-monotonic variation with the blockage. Although it was not explicitly stated, non-monotonic variation of L with B can be observed from figure 11 in the paper by Fornberg (1991). Using the towing tank boundary condition, L and θ_s increase with the blockage for small values of B. Beyond a critical blockage, a decrease in both the parameters with increasing B is observed. In contrast, the variation of L and θ_s with B is associated

with multiple regimes of non-monotonicity when the slip boundary condition is used. The non-monotonic variation of L and θ_s with B arises due to the non-monotonic movement of the separation point with the blockage. For $B \leqslant 0.01$, L and θ_s are free from the blockage effect. For high blockage, compared to the slip boundary condition, the towing tank condition leads to significantly larger acceleration of the flow near the cylinder. Also, the vorticity generated at the sidewalls with the towing tank boundary condition interferes with the advection of the vorticity generated on the surface of the cylinder. The outcome is a delayed flow separation and, therefore, a shorter bubble with the towing tank boundary condition. For large blockage, compared to the towing tank boundary condition, the results predicted by the slip boundary condition for the bubble dimensions are closer to the ones for the unbounded flow. For $B \leqslant 0.04$, both the boundary conditions yield very comparable results.

The values of Re_s from the present computations, for each blockage, exhibit close agreement with the value obtained via the criterion proposed by Srinivasan (2006). Also, excellent agreement is found with the predictions of Chen (2000) for $0.10 \leqslant B \leqslant 0.70$, using the towing tank boundary condition. For $B \leqslant 0.01$, Re_s is insensitive to the blockage. In general, Re_s obtained with the slip boundary condition are closer to the ones for the unbounded flow than those obtained with the towing tank boundary condition. Therefore, the use of the slip boundary condition is recommended for computation of flows if one is forced to use high blockage ($B > 0.17$) to predict the unbounded flow characteristics.

The variation of various flow parameters with Re has been studied for the unbounded flow, and empirical relations via curve fit have been proposed. The bubble length varies as $L = -0.847 + 0.1336\ Re$ for $Re_s < Re \leqslant 40$. The flow separation angle follows the relation $\theta_s = 77.66 - 152.65\ Re^{-0.5}$ for $10 \leqslant Re \leqslant 40$. The total drag coefficient is expressed as $C_d = 0.26 + 7.89\ Re^{-0.5}$ for $15 \leqslant Re \leqslant 40$. The pressure drag coefficient varies as $C_{dp} = 0.583 + 4.311\ Re^{-0.64}$ for $6 \leqslant Re \leqslant 40$. The empirical equation for the viscous drag coefficient is expressed as $C_{dv} = -0.016 + 4.938\ Re^{-0.60}$ for $6 \leqslant Re \leqslant 40$. The empirical equation for the base suction is found to be – $C_{pb} = 0.413 + 2.627\ Re^{-1}$ for $6 \leqslant Re \leqslant 40$. The maximum vorticity on the cylinder surface obeys the relation $\omega_{max} = -0.2284 + 0.9430\ Re^{0.5}$ for $6 \leqslant Re \leqslant 40$. The extrapolated results for L, C_d, C_{dp}, C_{dv} and ω_{max} match quite well with the numerical results from the literature for the steady flow at higher Re. In almost all cases, the proposed relations offer better agreement with the available experimental and computational data as compared to the equations proposed earlier.

REFERENCES

Acrivos, A., Leal, L. G., Snowden, D. D. & Pan, F. 1968 Further experiments on steady separated flows past bluff objects. *J. Fluid Mech.* **34**, 25–48.

Acrivos, A., Snowden, D. D., Grove, A. S. & Peterson, E. E. 1965 The steady separated flow past a circular cylinder at large Reynolds numbers. *J. Fluid Mech.* **21**, 737–760.

Allen, D. N. & Southwell, R. V. 1955 Relaxation methods applied to determine the motion in two dimensions of a viscous fluid past a fixed cylinder. *Quart. J. Mech. Appl. Math.* **8**, 129–145.

Apelt, C. J. 1961 The steady flow of a viscous fluid past a circular cylinder at Reynolds numbers 40 and 44. *Aeronaut. Res. Counc. Lond.* R & M **3175**, 1–28.

Brooks, A. N. & Hughes, T. J. R. 1982 Streamline upwind/Petrov–Galerkin formulations for convection dominated flows with particular emphasis on the incompressible Navier–Stokes equations. *Comput. Methods Appl. Mech. Engng* **32**, 199–259.

Chen, J. H. 2000 Laminar separation of flow past a circular cylinder between two parallel plates. *Proc. Natl Sci. Counc. ROC* A **24**, 341–351.

Coutanceau, M. & Bouard, R. 1977 Experimental determination of the main features of the viscous flow in the wake of a circular cylinder in uniform translation. Part 1. Steady flow. *J. Fluid Mech.* **79**, 231–256.

Dennis, S. C. R. & Chang, G. Z. 1970 Numerical solutions for steady flow past a circular cylinder at Reynolds numbers up to 100. *J. Fluid Mech.* **42**, 471–489.

Dennis, S. C. R. & Shimshoni, M. 1965 The steady flow of a viscous fluid past a circular cylinder. *Aero. Res. Counc. Current Papers*, no. 797.

Fornberg, B. 1980 A numerical study of steady viscous flow past a circular cylinder. *J. Fluid Mech.* **98**, 819–855.

Fornberg, B. 1985 Steady viscous flow past a circular cylinder up to Reynolds number 600. *J. Comput. Phys.* **61**, 297–320.

Fornberg, B. 1991 Steady incompressible flow past a row of circular cylinders. *J. Fluid Mech.* **225**, 655–671.

Gajjar, J. S. B. & Azzam, N. A. 2004 Numerical solution of the Navier–Stokes equations for the flow in a cylinder cascade. *J. Fluid Mech.* **520**, 51–82.

Ghia, K. N., Ghia, U., Osswald, G. A. & Liu, C. A. 1986 Simulation of separated flow past a bluff body using Navier-Stokes equations. In *Proc. of the IUTAM Symp. on Boundary Layer Separation.* London.

Grove, A. S., Shair, F. H., Peterson, E. E. & Acrivos, A. 1964 An experimental investigation of the steady separated flow past a circular cylinder. *J. Fluid Mech.* **19**, 60–80.

Hamielec, A. E. & Raal, J. D. 1969 Numerical studies of viscous flow around circular cylinders. *Phys. Fluids* **12**, 11–17.

Henderson, R. D. 1995 Details of the drag curve near the onset of vortex shedding. *Phys. Fluids* **7**, 2102–2104.

Homann, F. 1936 Einfluss grösser Zähigkeit bei Strömung um Zylinder. *Forsch. Ing. Wes.* **7**, 1–10.

Hughes, T. J. R. & Brooks, A. N. 1979 A multi-dimensional upwind scheme with no crosswind diffusion. In *Finite Element Methods for Convection Dominated Flows* (ed. T. J. R. Hughes), pp. 19–35. ASME.

Hughes, T. J. R., Franca, L. P. & Balestra, M. 1986 A new finite element formulation for computational fluid dynamics. Part 5. Circumventing the Babuška–Brezzi condition: a stable Petrov–Galerkin formulation of the Stokes problem accommodating equal-order interpolations. *Comput. Methods Appl. Mech. Engng* **59**, 85–99.

Kawaguti, M. 1953 Numerical solution of the Navier–Stokes equations for the flow around a circular cylinder at Reynolds number 40. *J. Phys. Soc. Jpn* **8**, 747–757.

Kawaguti, M. & Jain, P. 1966 Numerical study of a viscous fluid flow past a circular cylinder. *J. Phys. Soc. Jpn* **21**, 2055–2062.

Keller, H. B. & Takami, H. 1966 Numerical studies of viscous flow about cylinders. In *Numerical Solutions of Nonlinear Differential Equations* (ed. D. Greenspan), pp. 115–140. Wiley.

Kumar, B. & Mittal, S. 2006*a* Effect of blockage on critical parameters for flow past a circular cylinder. *Intl J. Numer. Methods Fluids* **50**, 987–1001.

Kumar, B. & Mittal, S. 2006*b* Prediction of the critical Reynolds number for flow past a circular cylinder. *Comput. Methods Appl. Mech. Engng* **195**, 6046–6058.

Mittal, S. 2000 On the performance of high aspect ratio elements for incompressible flows. *Comput. Methods Appl. Mech. Engng* **188**, 269–287.

Nieuwstadt, F. & Keller, H. B. 1973 Viscous flow past circular cylinders. *Comput. Fluids* **1**, 59–71.

Nishioka, M. & Sato, H. 1974 Measurements of velocity distributions in the wake of a circular cylinder at low Reynolds numbers. *J. Fluid Mech.* **65**, 97–112.

Nisi, H. & Porter, A. W. 1923 On eddies in air. *Phil. Mag.* **46**, 754–768.

Posdziech, O. & Grundmann, R. 2007 A systematic approach to the numerical calculation of fundamental quantities of the two-dimensional flow over a circular cylinder. *J. Fluids Struct.* **23**, 479–499.

Prasanth, T. K., Behara, S., Singh, S. P., Kumar, R. & Mittal, S. 2006 Effect of blockage on vortex-induced vibrations at low Reynolds numbers. *J. Fluids Struct.* **22**, 865–876.

Pruppacher, H. R., Clair, B. P. Le & Hamielec, A. E. 1970 Some relations between drag and flow past a sphere and a cylinder at low and intermediate Reynolds numbers. *J. Fluid Mech.* **44**, 781–790.

Saad, Y. & Schultz, M. 1986 GMRES: a generalized minimal residual algorithm for solving nonsymmetric linear systems. *SIAM J. Sci. Stat. Comput.* **7**, 856–869.

Sahin, M. & Owens, R. G. 2004 A numerical investigation of wall effects up to high blockage ratios on two-dimensional flow past a confined circular cylinder. *Phys. Fluids* **16**, 1305–1320.

Singh, S. P. & Mittal, S. 2005 Flow past a cylinder: shear layer instability and drag crisis. *Intl J. Numer. Methods Fluids* **47**, 75–98.

Smith, F. T. 1979 Laminar flow of an incompressible fluid past a bluff body: the separation, reattachment, eddy properties and drag. *J. Fluid Mech.* **92**, 171–205.

Smith, F. T. 1981 Comparisons and comments concerning recent calculations for flow past a circular cylinder. *J. Fluid Mech.* **113**, 407–410.

Sobey, I. J. 2000 *Introduction to Interactive Boundary Layer Theory*. Oxford University Press.

Son, J. S. & Hanratty, T. J. 1969 Numerical solution for the flow around a cylinder at Reynolds numbers of 40, 200 and 500. *J. Fluid Mech.* **35**, 369–386.

Srinivasan, K. 2006 On a separation criterion for symmetric elliptic bluff body flows. http://arxiv.org/pdf/physics/0511250.

Takami, H. & Keller, H. B. 1969 Steady two-dimensional viscous flow of an incompressible fluid past a circular cylinder. *Phys. Fluids Suppl.* **12**, II 51–II 56.

Taneda, S. 1956 Experimental investigation of the wakes behind cylinders and plates at low Reynolds numbers. *J. Phys. Soc. Jpn* **11**, 302–307.

Tezduyar, T. E., Mittal, S., Ray, S. E. & Shih, R. 1992 Incompressible flow computations with stabilized bilinear and linear equal-order-interpolation velocity–pressure elements. *Comput. Methods Appl. Mech. Engng* **95**, 221–242.

Thom, A. 1933 The flow past circular cylinders at low speeds. *Proc. R. Soc. Lond.* A **141**, 651–669.

Thoman, D. C. & Szewczyk, A. A. 1969 Time-dependent viscous flow over a circular cylinder. *Phys. Fluids Suppl.* **12**, II 76–II 86.

Tomotika, S. & Aoi, T. 1950 The steady flow of viscous fluid past a sphere and circular cylinder at small Reynolds numbers. *Quart. J. Mech. Appl. Math.* **3**, 140–161.

Tritton, D. J. 1959 Experiments on the flow past a circular cylinder at low Reynolds numbers. *J. Fluid Mech.* **6**, 547–567.

Tuann, S. Y. & Olson, M. D. 1978 Numerical studies of the flow around a circular cylinder by a finite element method. *Comput. Fluids* **6**, 219–240.

Underwood, R. L. 1969 Calculation of incompressible flow past a circular cylinder at moderate Reynolds numbers. *J. Fluid Mech.* **37**, 95–114.

Wu, M. H., Wen, C. Y., Yen, R. H., Weng, M. C. & Wang, A. B. 2004 Experimental and numerical study of the separation angle for flow around a circular cylinder at low Reynolds number. *J. Fluid Mech.* **515**, 233–260.

Yamada, H. 1954 On the slow motion of viscous liquid past a circular cylinder. *Rep. Res. Inst. Appl. Mech. Kyushu Univ.* **3**, 11–23.

Zdravkovich, M. M. 1997 *Flow Around Circular Cylinders*, vol. 1. Oxford University Press.